Universal Journal of Carbon Research
https://ojs.wiserpub.com/index.php/ujcr/

Review

Growth of Single-Walled Carbon Nanotubes from Solid Supported Heterogeneous Catalysts: Achievements and Challenges

Qianru Wu[1,2], Ningning Xu[1], Xinyan Chi[1], Wenjing Zhang[1], Kezheng Chen[2*], Maoshuai He[1*]

[1]College of Chemistry and Molecular Engineering, Qingdao University of Science and Technology, Qingdao, 266042, China
[2]College of Materials Science and Engineering, Qingdao University of Science and Technology, Qingdao, 266042, China
E-mail: hemaoshuai@qust.edu.cn

Received: 22 November 2023; **Revised:** 20 December 2023; **Accepted:** 21 December 2023

Abstract: Single-walled carbon nanotubes (SWNTs) have gained worldwide attention because of their exceptional electronic, optical, and mechanical properties, which are contingent on their structures denoted by chiral indices (n, m). To fully harness the extraordinary properties and advance SWNT-based technology, large scale synthesis of SWNTs with a narrow chirality distribution or even a specific (n, m) is highly demanded. Among various SWNT preparation techniques, chemical vapor deposition growth from solid supported heterogeneous catalysts has emerged as a promising approach in terms of large yield and (n, m) structure control. In this review, we provide an overview of the progress in developing heterogeneous catalysts for bulk synthesis of SWNTs. Firstly, the advantages and disadvantages of using solid supported catalysts for chemical vapor deposition growth of SWNTs are discussed. Secondly, the key components in supported catalysts, including the metallic component and the nature of support material, as well as their respective roles in affecting the catalyst performances and SWNT chirality distribution, are highlighted. Finally, the current challenges and future directions in the field of SWNT synthesis from solid supported catalysts are proposed.

***Keywords*:** single-walled carbon nanotubes (SWNTs); solid supported catalysts; catalyst performance; chemical vapor deposition; chirality control

1. Introduction

Single-walled carbon nanotubes (SWNTs) are an allotrope of sp^2 hybridized carbon comprised of 6-membered carbon rings[1]. They can be envisioned as one-dimensional hollow cylinders made from wrapping monolayer graphene with one atom thick wall[2]. The SWNTs generally have diameters smaller than 5.0 nm and most of them are in the diameter range of 0.7-2.0 nm[3, 4]. Based on the differences in rolling vector and lattice orientation, SWNTs are discriminated with different chiral indices (n, m). **Figure 1a**&**1b** presents the chiral vector and the structure of a (6, 5) nanotube, the diameter and chiral angle of which could be deduced from the vector. Depending on the vector directions or the chiral angles (**Figure 1c**), SWNTs could be classified into zigzag ones ($m = 0$, $\alpha = 0^o$), chiral ones ($n \neq m$, $0^o < \alpha < 30^o$), and armchair ones ($n = m$, $\alpha = 30^o$)[5]. Because of the dimensional constraints and unique chemical structure, SWNTs exhibit exceptional mechanical, electronic and optical properties, which render them attractive for a wide range of applications, including electronics[6], energy storage[7], sensors[8], and composites[9]. However, most of the intrinsic properties of SWNTs are sensitive to the SWNT chirality. For example, SWNTs demonstrate metallic properties if (n-m) could be divided by 3. Otherwise, SWNTs exhibit semiconducting properties, and the energy bandgap is inversely proportional to the

DOI: https://doi.org/10.37256/1220233904

SWNT diameter. Therefore, to realize their irreplaceable killer applications, it is of great importance to prepare SWNTs with desirable structures and properties.

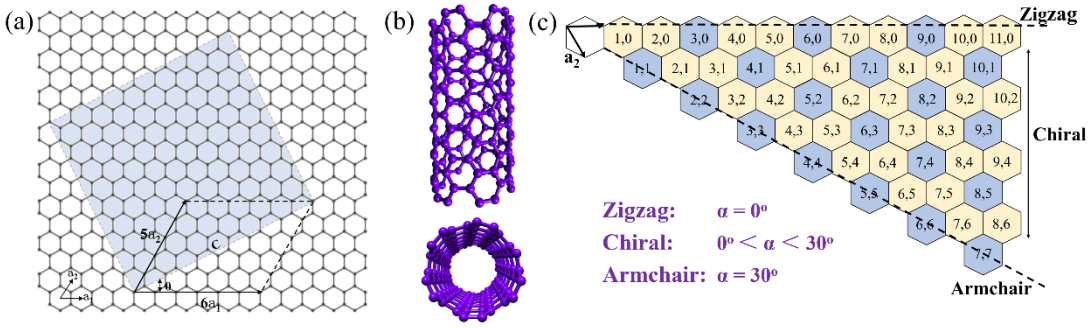

Figure 1. (a) Chiral vector and (b) structure of a (6, 5) nanotube. (c) Periodic table of SWNTs

Over the past 30 years, various methods, including arc discharge[10, 11], laser ablation[12], and chemical vapor deposition (CVD)[13], have been applied for synthesizing SWNTs. As the oldest technique for producing carbon nanomaterials, CVD has become the most widely used method for efficient growth of SWNTs with controlled properties[2, 14, 15]. A CVD process involves complex chemistry, and consists of both gas-phase and surface reactions. Volatile carbon precursor molecules transport into the reaction zone, and decompose or react with other reaction gases to form active carbon atoms, which subsequently absorb on the catalyst surfaces to form SWNT nuclei[16]. Further incorporation of carbon atoms to the SWNT-catalyst interface leads to the growth of SWNTs. In this process, the catalyst not only facilitates the dissociation and diffusion of carbon atoms, but also serves as the template for SWNT growth[17]. Therefore, the choice of catalyst and its interaction with the carbon atoms play crucial roles in determining the SWNT structure.

According to the way the catalyst particle is introduced into the reaction zone for SWNT growth, CVD systems are classified into three types: floating catalyst CVD, surface growth, and solid supported catalyst CVD. **Figure 2a** shows the scheme of floating CVD for SWNT synthesis. In the process, both the catalyst and carbon precursors are fed continuously to a reactor with the assistance of carrier gas[4, 18, 19]. Upon heating, the catalyst precursors are decomposed into metal atoms and subsequently aggregate into nanoparticles in the gas phase. Together with carbon source decomposition, carbon absorption and diffusion on catalyst particles, SWNT nucleation and growth all take place at the reaction zone. After floating out of the hot reaction zone, SWNT growth terminates, and the synthesized SWNTs can be collected at the gas outlet. For a typical floating CVD, the SWNT growth duration only lasts a few seconds, as it is shorter than the residence time for all the abovementioned processes to occur. Floating catalyst CVD is a promising technique for scalable synthesis of SWNTs and possesses several advantages. First of all, as the SWNTs are generated in gas phase, they are free of support materials; Secondly, the SWNTs float out of the hot zone after reaction, and therefore could be deposited onto various targeted substrates at low temperature zone, facilitating the subsequent applications of SWNT thin films in different fields[20]. Thirdly, the reaction temperature could be high enough to guarantee a high graphitization degree of SWNTs. For instance, the well-known commercial HiPco SWNTs, which have been widely used for fundamental research, are produced by the floating catalyst CVD method at a reaction temperature of 1050 °C[4]. The produced SWNTs exhibit an intensity ratio between G mode and D mode higher than 20.0 in the Raman spectra, indicative of well crystallized SWNTs[21]. However, the approach also suffers some drawbacks, such as the low catalyst efficiency, and the SWNT surface contamination by inactive catalyst particles. More importantly, as the catalyst is formed randomly in the gas phase during the precursor decomposition process, little control could be exerted over the size or structure of the catalyst particles. Consequently, the generated catalysts usually demonstrate a wide diameter distribution, and report on the diameter- or structure-controlled synthesis of SWNTs by the floating catalyst CVD is scarce[22].

Surface growth, which involves the dispersion/deposition of discrete nanoparticles or thin film catalyst on flat substrate[23, 24], affords the growth of SWNTs from the catalyst by CVD (**Figure 2b**). Initially, discrete SWNTs, the diameters of which are correlated with those of catalyst particles, are synthesized on different planar substrates, such as silica (SiO_2)[23, 25], magnesia (MgO)[26] and sapphire surfaces[27]. Owing to the negligible interference from neighboring carbon nanotubes during SWNT elongation process on surfaces, the quality of SWNTs is rather high, and field effect transistors made from semiconducting SWNTs demonstrate fascinating characteristics[28, 29]. In addition, the orientations of discrete SWNTs could be guided by the underlying substrate[30, 31] or the gas flow[32, 33], favoring the synthesis of horizontally aligned products. More importantly,

the chirality of SWNTs could be well tuned by the catalyst or molecular template, resulting in SWNTs with a single-chirality purity higher than 90%[34, 35]. Nevertheless, the poor SWNT yield and the SWNT nonuniformity on the whole substrate surface are the major hurdles for their practical applications. To improve the SWNT yield, highly dense nanoparticles or thin catalyst films are sputtered on the flat substrates for CVD synthesis. Under optimal reaction conditions, vertically aligned SWNT forests longer than several millimeters could be synthesized[24]. Although the SWNT growth efficiency is very high, the random cracking of metal film poses no constrains on the sizes of generated nanoparticles, leading to the synthesis of SWNTs with a broad diameter distribution. Moreover, owing to the interferences of elongating SWNTs with different growth rates during the growth process, most SWNTs are very defective, which deteriorates their intrinsic optical and electrical properties[24].

Solid supported catalyst CVD could bridge the precise control over (n, m) structure and bulk synthesis of SWNTs[36, 37]. The supported heterogeneous catalyst consists of oxide carriers and active catalyst components. Besides high thermal and mechanical stability, the mesoporous support carriers have large surface area, which provides sufficient sites for stabilizing the dispersed metal and regulating the catalyst performances, as schematically illustrated in **Figure 2c**. Similar to surface growth of SWNTs with high chirality selectivity, the solid supported catalyst could regulate SWNT (n, m) structures by controlling the catalyst-SWNT interface properties[38], which sheds light on large quantity synthesis of SWNTs with a narrow chirality distribution, thus paving the way towards single chirality SWNT preparation through post-growth separation approaches for high-tech applications. Although there are several reviews dedicated to the controlled growth and sorting of SWNTs[2, 39-41], a comprehensive summary of SWNT growth from solid-supported heterogeneous catalysts is currently lacking.

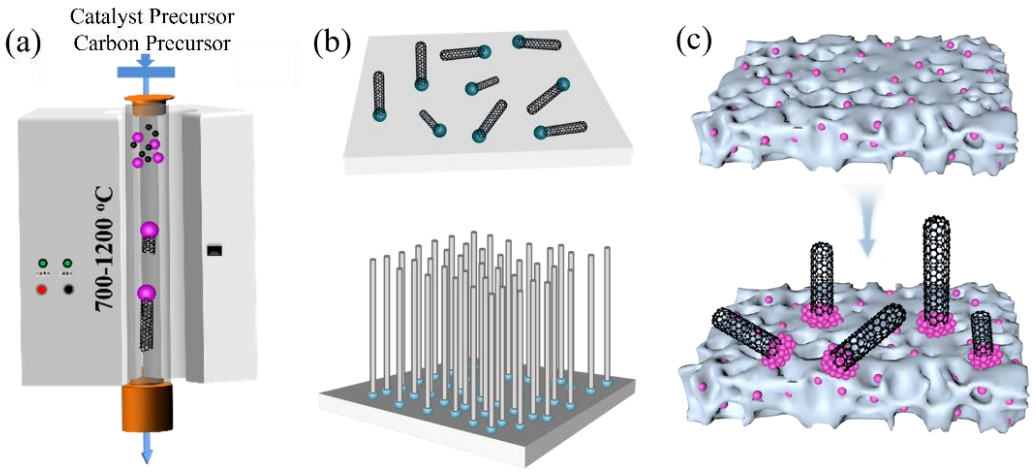

Figure 2. (a) Scheme of SWNT synthesis from floating catalyst CVD. (b) Schematic illustration of surface growth of SWNTs from discrete nanoparticles or metal thin films deposited on flat surfaces. (c) Scheme of growing SWNTs from solid supported catalyst CVD

In this review, the development history of solid support catalyst CVD for SWNT growth is firstly described. Pioneer reports on chirality selective synthesis of SWNTs from solid supported heterogenous catalysts are addressed. Secondly, the key roles of the catalyst in determining SWNT nucleation and growth kinetics are briefly discussed. Thirdly, different catalysts, classified by active components and support materials, are respectively discussed. Finally, the challenges and prospects in synthesizing SWNTs from solid support catalysts are proposed.

2. History of solid supported catalysts in SWNT synthesis

The discovery and development of carbon nanotubes have a rich history. While credit for the formal discovery in 1991 is given to Sumio Iijima, who observed carbon nanotubes as byproducts during electric arc experiments for fullerenes deposition[42], it is also important to acknowledge the work of Radushkevich and Lukyanovich[43], who published transmission electron microscopy (TEM) images clearly showing carbon fibers with a continuous inner cavity in 1952[44]. To synthesize SWNTs, catalyst particles with suitable diameters are required during the reaction process. The first growth of SWNTs using electric arc experiments involved filling of graphite rods with Fe or Co metal, resulting in independent syntheses by two research groups in 1993[10, 11]. In 1996, Dai and co-workers made an important advancement by developing a molybdenum (Mo) catalyst supported by fumed alumina nanoparticles for CVD synthesis by disproportionation of carbon monoxide (CO)[45].

The reaction temperature was high (1200 °C), and the produced SWNTs exhibited diameters ranging from 1 to 5 nm. Subsequent work by Kong et al.[46] systematically investigated the synthesis of SWNTs on a variety of silica and alumina supported Fe-family metal catalysts by methane (CH_4) CVD. They discovered that the type of support controlled the bundle size of the produced SWNTs. Amorphous silica supported catalyst yielded bundled SWNTs, while crystalline alumina nanoparticle supported catalysts produced only individual SWNTs or small bundles. This research highlighted the critical roles of both the supported catalyst and the CH_4 carbon source in synthesizing SWNTs[43]. Compared with SiO_2 and alumina, MgO support could be removed more easily by mild acid treatment after reaction, therefore, great efforts have been made in designing MgO supported catalysts for SWNT synthesis[47, 48]. By reducing $Co_{0.1}Mg_{0.9}O$ solid solution in hydrogen-CH_4 atmosphere, Flahaut et al.[47] prepared carbon nanotubes with diameters of 0.5-5.0 nm, which are mixture of SWNTs and double-walled carbon nanotubes. High purity SWNTs grown from MgO supported *3d* transition metals were reported by Li et al. in 2001[48]. In their work, five kinds of oxide support were systematically investigated and only porous MgO was revealed to be suitable for metal incorporation to grow SWNTs. On a typical MgO-supported Fe catalyst, the choice of hydrocarbons was revealed to play an important role in CVD synthesis, with different hydrocarbons resulting in variations in the structure of the carbon deposits[49]. Specifically, aromatic molecules such as benzene and naphthalene tended to favor the synthesis of SWNTs. However, most of the synthesized SWNTs exhibited wide diameter distributions at this stage of research.

With the simultaneous advancements in SWNT characterizations by optical techniques, like UV-vis-NIR absorption spectroscopy and photoluminescence (PL) spectroscopy[50, 51], chirality selective synthesis of SWNTs with enrichment of specific (n, m) species began to flourish. Bachilo et al.[36] employed PL spectroscopy to analyze the SWNTs produced by the disproportionation of CO on a silica supported CoMo catalyst. They revealed that more than half of the semiconducting SWNTs synthesized were the (6, 5) and (7, 5) chirality. Compared with HiPco SWNTs generated by floating CVD[4], the SWNTs synthesized on the CoMo/silica catalyst exhibited a much narrower chirality distribution. Similarly, Maruyama et al.[52] used fluorescence spectroscopy to characterize SWNTs synthesized on a zeolite supported FeCo catalyst. The SWNTs grown *via* alcohol CVD demonstrated enrichment of (7, 5) and (7, 6) species, and their chirality distribution was also narrower than that of HiPco SWNTs. These pioneer works marked the beginning of chirality-selective synthesis of SWNTs using solid support catalyst. The exploration of key factors influencing SWNT chirality distribution will be detailed in the following sections.

3. SWNT chirality distribution dependence on CVD parameters

In theory, all the parameters related to CVD growth process, including reaction temperature, pressure, carbon source, catalyst size and component, can influence the structures of synthesized SWNTs.

3.1 *Reaction temperature*

The typical reaction temperature for CVD growth of SWNTs ranges from 400 to 1200 °C. Generally, higher reaction temperature tends to increase the graphitization degree of the SWNTs, thus promoting the synthesis of high quality SWNTs with excellent properties. However, elevated reaction temperature can also lead to the coalescence and sintering of reduced metal particles[53], resulting in the formation of large diameter SWNTs or even multi-walled carbon nanotubes. Another factor contributing to temperature-dependent chirality distribution is the entropy-driven stability of chiral SWNTs on the catalyst surface[54], and high reaction temperature is generally unfavorable for controlling SWNT chirality. Therefore, to narrow the SWNT chirality distribution, most reactions are constrained to low temperature CVD growth[37, 53]. For example, the reaction temperature for producing commercial CoMoCAT SWNTs, enriched in (6, 5) SWNTs, is set below 750 °C[55]. Similarly, the predominant synthesis of (6, 5) SWNTs has been achieved at about 600 °C in various studies[37, 53, 56, 57]. For example, an MgO supported FeCu catalyst facilitated the growth of SWNTs with higher yield than monometallic Fe catalyst. In the bimetallic catalyst, the presence of Cu promoted the reduction and activation of Fe at low reaction temperature, partially contributing to the dominant synthesis of (6, 5) SWNTs[37, 58]. The findings are consistent with numerous other reports[52, 54, 55], which disclosed that decreasing reaction temperature leads to a narrower SWNT chirality distribution.

In typical CVD process, synthesizing SWNTs at temperatures lower than 600 °C is challenging due to the presence of the energy barriers for carbon source dissociation and nanotube nucleation. However, for compatibility with the CMOS technology, which permits a maximum temperature of 450 °C, it is imperative to minimize the growth temperature as much as possible[59]. In 2011, He et al.[60] introduced a silica supported Ni catalyst for low temperature growth of SWNTs. The H_2-temperature programmed reduction (H_2-TPR) profile of

the catalyst suggested that reduction commenced at about 400 °C, correlated to the activation of the Ni particles. As a result, SWNTs could grow on the Ni/SiO_2 catalyst at 450 °C, and high quality ones were synthesized at 500 °C, as indicated by the relatively low intensity of D mode in the Raman spectra[60].

On the contrary, a higher reaction temperature is preferred for synthesizing SWNTs with elevated graphitization degree. To achieve this while maintaining the narrow SWNT chirality distribution, it becomes essential to prepare supported catalysts with robust metal-support interaction. A strong metal-support interaction not only aids in anchoring the reduced metal nanoparticles but also minimizes the nonuniformity of active catalysts, thus favoring chirality selection during high-temperature CVD. In 2022, Wu et al.[61] designed an MgO supported Co catalyst using a simple impregnation technique. Environmental transmission electron microscopy (ETEM) revealed that metallic Co nanoparticles were generated on the MgO surface at 700 °C in a reducing CO atmosphere. No particle coalescence was observed with prolonging the reaction time. The ETEM analysis indicated a strong metal-support interaction between the reduced Co and the underlying MgO support. This is because the surface vacancies on the MgO surface act as the anchoring sites for stabilizing reduced Co nanoparticles. As a result, high quality SWNTs with a narrow chirality distribution were synthesized at a high temperature of 800 °C, with only a few major species, like (6, 5), (7, 5), (8, 3) and (8, 4) detected by PL. Moreover, thermogravimetric analysis (TGA) of the purified SWNTs revealed an oxidation peak of approximately 476 °C[61], higher than that of SWNTs grown at lower temperatures. This work shows the potential of high temperature growth of SWNTs with a narrow chirality distribution.

3.2 *Carbon precursor*

The type of carbon precursor is coherently related to the chirality distribution of SWNTs. Although various hydrocarbons were initially explored for growing SWNTs in early reports[49], the prevalent carbon sources for chiral-selective synthesis of SWNTs have been mainly limited to ethanol[52], CH_4[57] and CO[62]. Among them, ethanol stands out as an environmentally friendly carbon source, characterized by its non-toxic nature and minimal environmental impact even in the event of spillage. Alcohol CVD (ACCVD) was initially developed and extensively investigated by Maruyama's research group at the University of Tokyo[52, 63, 64]. In the ACCVD process, the heterogeneous catalyst adopted is a USY-zeolite supported FeCo catalyst[52]. Owing to the presence of OH radicals, which result from the decomposition of ethanol, the formation of impurities such as amorphous carbon and carbon nanoparticles is effectively suppressed, leading to the growth of high purity SWNTs. The suppression effect is attributed to the etching effect of the OH radicals, which tend to attack carbon atoms with dangling bonds. By using isotopically labeled ethanol ($^{12}CH_3$–$^{13}CH_2$–OH), researchers were able to track the carbon atoms during SWNT formation process[65]. In addition to producing ethylene by gas-phase decomposition, ethanol molecules themselves interact with the catalyst surface and participate in SWNT growth. Interestingly, carbon atoms located away from the hydroxyl group are preferentially incorporated into the SWNT structure, and this process is sensitive to the reaction temperature and the catalyst component. Consequently, by tuning the catalyst composition, it is possible to regulate ethanol dissociation and consequently control the chirality distribution of SWNTs.

As ethanol is in a liquid state under ambient conditions, carrier gases are usually required to transport ethanol molecules into the reaction zone. From this point of view, gaseous carbon precursors offer more convenience for introduction into the CVD reactor. CH_4, the primary component of natural gas, has been widely adopted as the carbon source in bulk synthesis of SWNTs, which usually exhibit a broad diameter distribution[48, 55]. In 2007, Li et al.[57] demonstrated CH_4 CVD for selective synthesis of (6, 5) SWNTs on a silica supported bimetallic FeRu catalyst at 600 °C. In comparison to CoMoCAT SWNTs exhibiting a high preference for (6, 5) tubes, the CH_4 grown SWNTs exhibited a similar concentration of (6, 5) species. In 2017, Xu et al.[66] reported the preferential synthesis of (6, 4) SWNTs by finely controlling the oxidation degree of zeolite supported Co catalyst through CH_4 CVD. It is worth noting that in this work, plasma irradiation was supplied using radiofrequency-powered coils, leading to the dissociation of CH_4 in a manner distinct from thermal CVD. The wide availability and cost-effectiveness render CH_4 an ideal carbon source for chiral-selective synthesis of SWNTs. Additionally, the high H/C ratio of CH_4 leads to the generation of H_2 by thermal decomposition, which can serve as etching agents for removing the amorphous carbon coating on catalyst surface. This, in turn, extends the lifetime of the catalyst particle and increases SWNT growth efficiency[49, 67]. However, the presence of reducing H_2 at reaction temperature inevitably causes the coalescence of metal catalyst, potentially degrading SWNT diameter and chirality control.

Similar to CH_4, CO is thermodynamically stable in the absence of catalyst under reaction conditions. The disproportionation of CO is known as the Boudouard reaction, which is exothermic at all temperatures and leads to the formation of carbon dioxide (CO_2) and graphite. At temperatures higher than 700 °C, the forward reaction

is thermodynamically unfavored[68]. In addition, the CO_2 generated from CO disproportionation is a weak oxidizing gas[69], and could help etch excessive carbon atoms on the catalyst surface. Consequently, adopting CO as the carbon precursor facilitates the growth of high purity SWNTs. In fact, commercially available SWNTs, such as CoMoCAT, HiPco and CANATU SWNTs[36, 70, 71], all deploy CO as the carbon source during their synthesis procedures. The comparison between CO and CH_4 was initially made by Lolli et al.[55], who investigated the SWNT growth on the CoMoCAT catalyst through varying the gas feed. **Figure 3a** presents UV-vis-NIR absorption spectra of the SWNTs produced at 800 °C. Obviously, CO-grown SWNTs exhibit a high selectivity for (6, 5) SWNTs, while SWNTs grown from CH_4 could not afford a narrow (n, m) distribution. Different kinetics, which are related to the byproducts of CH_4 dissociation (H_2) and CO disproportionation (CO_2), were proposed to be responsible for the different chirality distributions[55]. Using TEM and nanobeam electron diffraction, He et al.[72] examined SWNTs grown from discrete Fe nanoparticles using different carbon feeds. At a reaction temperature of 800 °C, thin SWNTs with a diameter range of 0.7-1.6 nm were produced by using CO as the carbon precursor. In contrast, large diameter SWNTs ranging from 1.0 to 4.7 nm were synthesized from CH_4. Moreover, the CO-grown SWNTs demonstrated a preference for large chiral angle SWNTs, while CH_4-grown SWNTs exhibited a randomly distributed chiral angle, likely due to the large structural diversity of the products. Further studies revealed that CO and CH_4 respectively facilitated the nucleation of SWNTs in perpendicular mode and tangential mode[73, 74], classified by the diameter ratio between the SWNT and the catalyst particle (**Figure 3b, 3c**). The SWNT/catalyst diameter ratio was found to be determined by the carbon concentration inside the metal catalyst. When the carbon content within the metal particle is low, the catalyst particle tends to wet the inner surface of nanotube, and the tangential configuration is thermodynamically stable[74]. At high carbon content, the metal particle dewets the inner tube wall. Consequently, a perpendicular mode, where the SWNT has a smaller diameter than the catalyst particle, is favored. Experimentally, the rate constant for Fe carburization originating from CO disproportionation at 800 °C is about 1.5×10^{-4} mol·cm^{-2}·s^{-1}·bar^{-1}, which is about two orders of magnitude larger than the CH_4 carburization rate (1.9×10^{-6} mol·cm^{-2}·s^{-1}·bar^{-1})[75]. As a result, the carbon content inside metal nanoparticles delivered by Boudouard reaction is relatively high, accounting for the perpendicular mode and narrow diameter distribution of SWNTs grown from CO carbon precursor. The preference to grow SWNTs by the perpendicular mode explains the extensive use of CO for growing small diameter SWNTs.

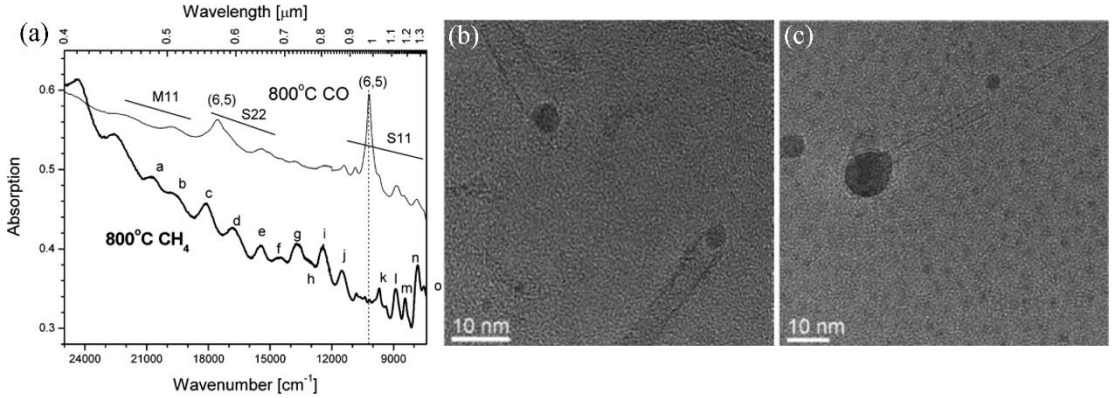

Figure 3. (a) UV-vis-NIR absorption spectra of the SWNTs produced on the CoMoCAT catalyst at 800 °C respectively using CO and CH_4 as the carbon source[55]. Copyright 2006 American Chemical Society. TEM images of SWNTs grown in (b) tangential mode from CH_4 and (c) perpendicular mode from CO[74]. Copyright 2018 Royal Society of Chemistry

3.3 *Reaction pressure*

The pressure of the carbon precursor significantly influences the nucleation and growth kinetics of SWNTs, and should be discussed in the context of carbon feed and reaction temperature. In typical ACCVD experiments, a constant pressure around 1 kPa is usually used to efficiently grow SWNTs within the temperature range of 600-800 °C[52]. In 2017, Hou et al.[64] investigated an extended pressure range for ACCVD on a zeolite-supported Fe-Co catalyst. They varied the partial pressure of ethanol within the temperature range of 350-900 °C, ranging from 0.02 Pa to 15 kPa. **Figure 4a** shows the comprehensive exploration on CVD conditions, with different colors and shapes denoting the G/D ratio deduced from Raman spectra. As identified by red crosses, there are two SWNT growth boundaries in the map. These boundaries showed a positive correlation between temperature and pressure. At an ethanol pressure of 0.02 Pa, SWNT growth was possible at a lower temperature of 430 °C (**Figure 4b**). However, such a low ethanol pressure could not support SWNT growth at temperatures higher than 700 °C. In

contrast, at an ethanol pressure of 10^4 Pa, high quality SWNTs could be synthesized at 900 °C. Furthermore, increasing the ethanol pressure resulted in a narrower SWNT diameter distribution (**Figure 4c**). This was interpreted by carbon overfeeding, selectively poisoning some catalyst through carbon encapsulation. The strategy of selective poisoning by excessive ethanol supply was also applied in the surface growth of (2n, n) SWNTs on solid catalysts[35], which have the most available kinks at the SWNT-catalyst interface[38]. As a result, increasing carbon supply could deactivate other SWNTs with fewer kinks and improve the chirality selectivity towards (2n, n) nanotubes[76].

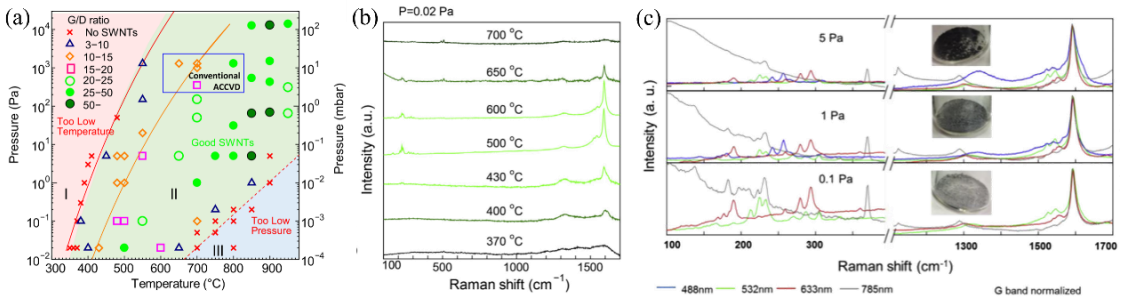

Figure 4. (a) A contour plot of ACCVD experimental map including all reaction information. (b) Raman spectra of samples grown from 370 °C to 700 °C at an ethanol pressure of 0.02 Pa. (c) Normalized Raman spectra of SWNTs grown from 0.1 Pa to 5 Pa ethanol at 480 °C. The spectra were acquired with four excitation laser wavelengths [64]. Copyright 2018 Royal Society of Chemistry

The influence of CO pressure on the SWNT synthesis from an MCM-41 supported Co catalyst was investigated by characterizing the synthesized SWNTs and Co nanoclusters[77]. **Figure 5a** presents Raman spectra recorded from SWNTs grown at 800 °C with different CO pressure. The intensities of radial breathing modes (RBMs) with higher frequencies, corresponding to SWNTs of smaller diameters, increase as the CO pressure rises. An absorption spectrum of SWNTs grown at a high CO pressure of 6 atm confirms a narrow chirality distribution. **Figure 5b** plots the total carbon yield as a function of the CO pressure, demonstrating that larger amounts of carbon deposits are produced at higher CO pressures. The results indicate strong correlations between CO pressure and SWNT selectivity and yield. Similar results were also reported by Wang et al.[78], who studied the selective growth of SWNTs by adjusting CO pressure in the range of 2 to 18 bar on a silica supported CoMo catalyst. **Figure 5c** illustrates PL emission maps of SWNTs synthesized at different CO pressure. In all the maps, dominant SWNT species are (6, 5), (7, 5), and (7, 6) with large chiral angles. Increasing CO pressure from 2 to 18 bar leads to the enrichment of small diameter (6, 5) tube, and a concentration of about 50% could be reached at 18 bar CO pressure. The increased abundance of (6, 5) tube is accompanied by the decreased concentration of large diameter (7, 6) type. The observations suggest that increasing the reaction pressure promotes the growth of (6, 5) SWNTs with a small diameter of 0.75 nm. It is speculated that increasing CO pressure increases the CO striking coefficient on Co nanoparticles, thus shortening the incubation time for SWNT nucleation, which minimizes the possibilities for Co nanoparticle sintering and nucleation of large diameter SWNTs[78]. Consequently, high pressure CO is widely adopted for selectively growing small diameter SWNTs[36, 55]. Nevertheless, considering the cost and safety issue of high-pressure reaction, CVD growth of SWNTs using ambient CO is highly desirable.

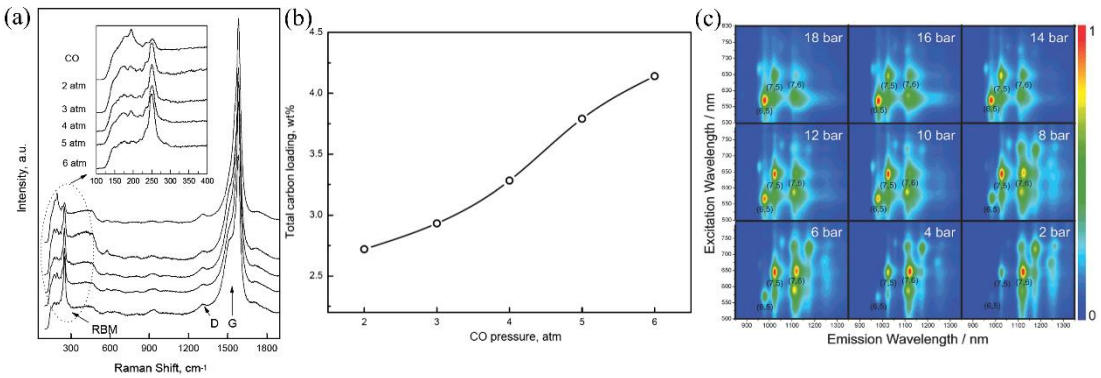

Figure 5. (a) Raman spectra recorded from SWNTs grown on MCM-41 supported Co catalyst at 800 ºC with different CO pressure. (b) Total carbon yield as a function of the CO pressure[77]. Copyright 2004 Elsevier. (c) PL emission maps of SWNTs synthesized at different CO pressure from a $CoMo/SiO_2$ catalyst at 800 ºC[78]. Copyright 2007 American Chemical Society

4. Heterogeneous catalysts for chiral selective synthesis of SWNTs

Based on the above discussions, it is summarized that the optimization of CVD parameters significantly influences the SWNT chirality distribution. Since SWNT growth takes place on the catalyst surface, the interface between SWNT and catalyst is pivotal for achieving selective synthesis. In solid supported heterogenous catalyst, the properties of both the support materials and the active metal components play crucial roles in regulating the catalyst performances. This section will begin by exploring how the catalyst influences SWNT growth results, followed by a discussion of various solid-supported catalyst systems categorized based on their active metal components.

4.1 *Effects of catalyst on SWNT synthesis*

4.1.1 *Effect of catalyst size*

While SWNT nucleation can occur through various modes, the size of the catalyst particle significantly influences the number of nanotube walls and diameters. Initial efforts in synthesizing SWNTs on flat substrate surfaces are mainly focused on the preparation of monodisperse nanoparticles. In 2001, Li et al.[79] reported the growth of SWNTs from Fe nanoparticles with diameters in the range of 1-2 nm and 3-5 nm, respectively. Using TEM, the authors, for the first time, presented both ends of an isolated SWNT, which revealed a diameter correlation between the SWNT and the catalyst particle. Consequently, controlling catalyst diameters enables the control of SWNT diameters. Similarly, by preparing nanoparticles with different average diameters, Cheung et al.[80] demonstrated the growth of carbon nanotubes with average diameters of 3, 7, and 12 nm, respectively. As the nanotube diameter increased, the number of walls increased from one to two or three. Subsequent efforts have been focused on designing uniform metal nanoparticles for growing SWNTs with consistent size and even chirality. For instance, An et al.[81] utilized molecular nanoclusters containing 84 Mo atoms and 30 Fe atoms as catalysts for CVD synthesis of SWNTs. Although the resulting SWNTs exhibited an average diameter of 1.0 nm, close to the original cluster diameter of 1.3 nm, they still possessed a wide diameter distribution (0.7 to 1.5 nm), due to the aggregation of a small number of nanoclusters. In 2022, Lv et al.[82] characterized the SWNTs synthesized from 1.4 nm Au clusters. Despite the uniform diameter of the Au clusters (1.4 nm), the diameters of CO-grown SWNTs ranged from 0.75 to 1.8 nm. Additionally, large-chiral-angle SWNTs were enriched in the products, explained by their fast kinetics on the basis of vapor-liquid-solid growth mechanism[82]. Ostwald ripening, driven by the low melting temperature of the catalyst particle in the reaction environment, led to diverse diameter distributions of SWNTs.

4.1.2 *Physical state of catalyst*

To control the diameter and chirality of SWNTs, it is imperative to develop solid templates with a uniform structure that enables the synthesis of SWNTs by the vapor-solid-solid mechanism. Solid templates applied for SWNT synthesis could be classified into two types: one involves utilizing various carbon segments that act as seeds for subsequent elongation of SWNTs during CVD, a process known as nanotube cloning. The pioneering example of SWNT amplification was reported by Smalley et al.[83]. In their work, SWNTs were initially cut into short segments with open ends, which were then functionalized to dock FeO nanoparticles. Upon reduction, the docked particles at the SWNT ends could be converted into active metal, catalyzing amplified growth through carbon feeding at high reaction temperatures. Using AFM, a long and straight bidirectionally grown SWNT, identical in diameter to the original SWNT, was traced, confirming the amplified growth from short SWNTs. Subsequently, Yao et al.[84] suggested using open ended SWNTs for continued SWNT growth without the addition of new catalyst. Raman characterizations revealed that the newly grown segment had the same diameter and chirality as the parent SWNTs. Other carbon segments, such as opened fullerene caps[85], sorted SWNTs[86], carbon nanorings[87], and ultrashort nanotube seeds[88] can also serve as seeds for SWNT cloning by vapor phase epitaxy. However, most of the processes suffer from low yields, limiting their practical application in the bulk synthesis of SWNTs.

Alternatively, a variety of catalyst nanoparticles with high melting temperatures, capable of preserving their solid state at reaction conditions, has been applied for the template growth of SWNTs with specific (n, m) structures. In 2014, Yang et al.[34] designed W_6Co_7 alloy nanoparticles for selectively growing (12, 6) SWNTs.

The presence of refractory W in the alloy imparts a high melting temperature to the catalyst particles, enabling the synthesis of SWNTs by vapor-solid-solid mechanism. Density functional theory (DFT) calculations showed that (12, 6) nanotube demonstrates a perfect geometrical match with the (0 0 12) plane of W_6Co_7 nanoparticle, and the thermodynamic ascendancy accounts for the chirality specific growth of SWNTs. As a results, it becomes feasible to control the SWNT (n, m) structure by regulating the crystalline plane for nucleating SWNTs[34]. However, the reconstruction of alloy nanoparticles was revealed to be complex under CVD reaction environment[89], making precise control of specific crystalline plane for growing nanotube extremely difficult. In 2017, Zhang et al.[35] designed several carbides for catalyzing the growth of horizontal arrays of (2n, n) SWNTs. Using Mo_2C (100) with a 6-fold symmetry as a catalyst, (12, 6) SWNTs with the same symmetry are favored to grow. Similarly, the WC(100) plane with a 4-fold symmetry facilitates the synthesis of (8, 4) tubes. In addition to symmetry matching, the fast growth kinetics of (2n, n) SWNTs also contribute to their enrichment, as later addressed by He et al.[90]. Despite the progress, the approaches are only applicable to the surface growth of SWNTs, which suffers from very low SWNT yield and is unsuitable for large quantity synthesis of SWNTs with high chirality selectivity.

4.1.3 *Composition of catalyst*

The catalyst composition has been identified as a significant factor influencing SWNT synthesis[91, 92]. Using DFT, Ding et al.[91] proposed that the adhesion between SWNTs and metal nanoparticle must be sufficiently strong to support the growth of nanotubes. Commonly used catalysts, such as Fe, Co and Ni, possess strong adhesion to SWNTs, stabilizing the open end and preventing the nanotube closure during growth. In contrast, late transition metals, like Cu, Pd, and Au, exhibit weak metal-SWNT adhesion, rendering theme unsuitable for efficient SWNT growth. Yazyev et al.[92] also investigated the impact of metal elements on the catalytic growth of carbon nanotubes through first-principles calculations. They revealed that the choice of catalyst could affect the carbon diffusion pathways and the stability of growing nanotubes. Although the binding of SWNTs through armchair edges are more energetically favorable, the stability varies significantly among the metals investigated, including Ni, Pd, Pt, Cu, Ag, and Au. Notably, Cu exhibits the lowest energy barrier for carbon diffusion, indicating that SWNT growth could occur at much lower reaction temperatures. Additionally, Cu was also suggested as the most promising catalyst for growing SWNTs of defined chirality.

However, experimental results often deviate from theoretical predictions[93, 94]. For example, Takagi et al.[93] demonstrated that metal particles within the size range of 1-3 nm, including Cu, Ag and Au, can act as catalysts for synthesizing SWNTs in CVD. The essential role of catalyst is believed to provide a platform for the self-assembled formation of a hemispherical cap. In 2008, Yuan et al.[94] demonstrated the growth of horizontally aligned SWNTs on quartz substrates from a large variety of metals, including Fe, Co, Ni, Cu, Pt, Pd, Mn, Mo, Cr, Sn, Au, Mg, and Al. To date, various nanoparticles containing metals, oxides, or carbides, have been employed for catalytic CVD growth of SWNTs on flat surfaces[34, 35, 57]. Unfortunately, systematic characterizations on SWNTs synthesized on different catalysts have been lacking, primarily due to the limited yield of SWNTs grown on flat surfaces.

4.2 *Solid supported heterogeneous catalysts for SWNT growth*

In contrast to flat substrates with smaller surface areas for catalyst anchoring and SWNT growth, solid supported heterogeneous catalysts offer the advantages of large surface area and high metal loading. These features facilitate large-scale synthesis of SWNTs, providing ample material for comprehensive characterizations. In the following sections, we will discuss solid supported heterogeneous catalysts applied for growing SWNTs, categorizing them based on the active catalyst components.

4.2.1 *Co-based catalysts*

One of the most successful catalyst systems for growing SWNTs with narrowly distributed chirality is the CoMoCAT[36], which consists of a silica support and CoMo metallic components. In the CoMoCAT process, SWNTs are produced at 700-950 ^oC with pure CO flow at a pressure range of 1-10 bar[95]. During the CVD process, the synergistic effect between Mo and Co is essential for determining catalyst performance, which is sensitive to the Mo:Co atomic ratio[96]. The catalyst is very active and selective for growing SWNTs only when there is sufficient Mo present. **Figure 6a** illustrates the evolutions of the respective metals. The interaction between Co and Mo improves the Co dispersion and hinders the sintering of reduced Co clusters. The stabilized Co nanoparticles act as active components for growing SWNTs. Excessive Co in the catalyst forms large particles, which produce undesirable carbon forms, such as multi-walled carbon nanotubes and graphitic layers[96]. Along

with the regulation of the reaction temperature and CO pressure, it is possible to respectively synthesize enriched (6, 5) or (7, 6) nanotubes on the CoMoCAT catalyst (**Figure 6b, 6c**).

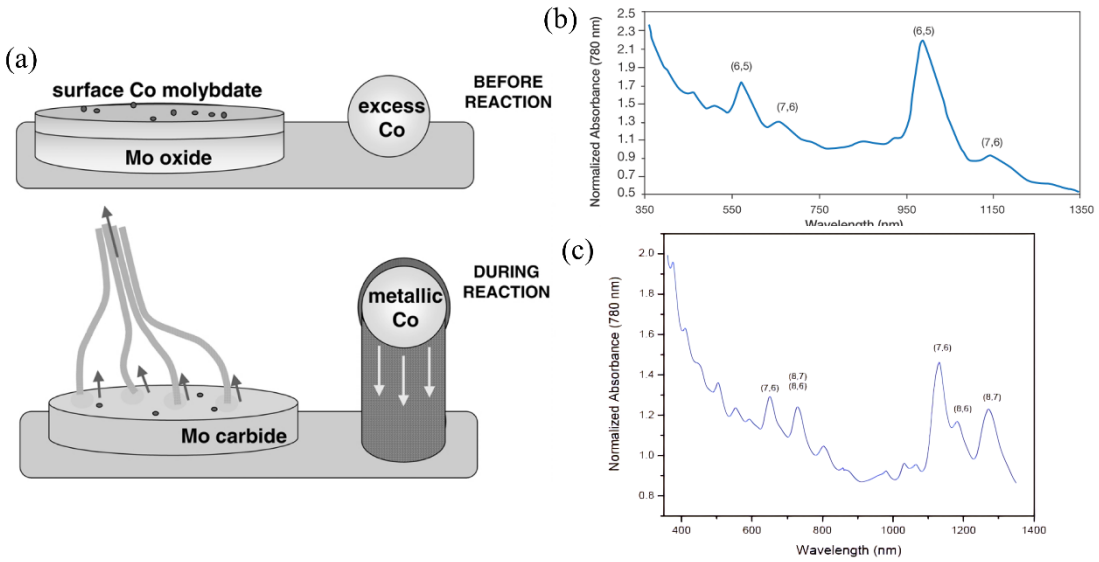

Figure 6. (a) Schematic representation of the state of the catalyst components before and during the production of SWNTs[95]. Copyright 2002 Kluwer Academic Publishers. (b-c) UV-vis-NIR absorption spectra of CoMoCAT SWNTs with enriched (6, 5) or (7, 5)

In the CoMoCAT process, the stabilization effect is derived from the surface CoMo-like structure. Disrupting this structure leads to the formation of molybdenum carbide and the release of small Co clusters. However, postgrowth removal of molybdenum carbide is challenging and typically requires the use of harsh hydrofluoric acid. To eliminate the need for Mo in the catalyst, several strategies have been proposed to stabilize reduced Co nanoclusters. One approach is to use a porous support with nanochannels, such as zeolite or MCM-41[97, 98], for incorporating Co ions. In 2003, Haller's group reported the synthesis of uniform SWNTs from Co-substituted MCM-41 molecular sieves with nanopores[97]. The Co ions were incorporated into the siliceous MCM-41 framework through a hydrothermal method. **Figures 7a** and **7b** show the nitrogen physisorption results of Co-MCM-41 using alkyl templates with different carbon chain lengths. The core size and corresponding pore volume increased linearly with the alkyl chain length C12-C18. After prereduction with H_2, SWNT growth was performed at 750 °C using 5 atm CO. **Figure 7c** presents UV-vis-NIR absorption spectra of SWNTs grown in C12 and C16 templates[98]. The inset is a TEM image of uniform SWNTs grown in the C12 template. All the SWNT diameters are smaller than the template pore diameters. The characterization results suggested that uniform SWNTs with narrow chirality distribution were synthesized from the monometallic Co-MCM-41. By analyzing extended X-ray absorption fine structure (EXAFS) spectra recorded for C12 and C16 samples after exposure to reaction conditions, the average coordination number and diameters of Co clusters were determined (**Figure 7d**)[98]. The Co clusters from reducing C12 and C16 samples contained fewer than 20 and 30 Co atoms, respectively. The uniform Co cluster size accounted for the growth of SWNTs with uniform diameters, demonstrating the potential of controlling SWNT structures by using mesoporous materials.

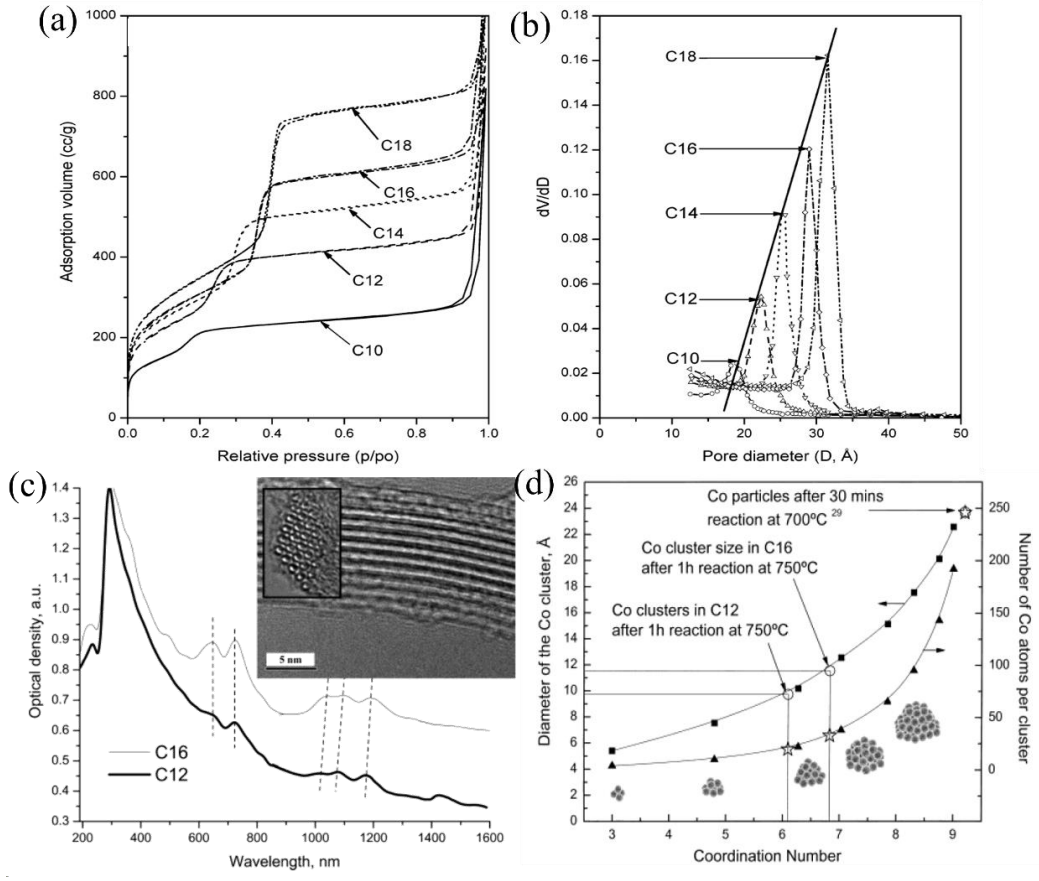

Figure 7. (a-b) Nitrogen physisorption results of Co-MCM-41 using alkyl templates with different carbon chain lengths[97]. Copyright 2003 American Chemical Society. (c) UV-vis-NIR absorption spectra of SWNTs grown in C12 and C16 templates. (d) Upper diameter limit of the Co clusters determined from the analysis of the EXAFS spectra [98]. Copyright 2004 American Chemical Society

However, practical applications of MCM-41 supported catalysts for synthesizing SWNTs are hampered by several drawbacks. Firstly, SWNTs grown from the MCM-41 supported catalyst do not exhibit a narrower chirality distribution compared to those from catalysts prepared by chemically grafting Co^{2+} ions on the silica outer surface[99-102]. Secondly, the MCM-41 mesoporous support is prohibitively expensive for real applications. An alternative approach involves anchoring reduced Co metal nanoparticles using metal cations in supported catalysts was thus proposed for the chiral selective synthesis of SWNTs. He et al.[99] employed ALD technique to create a silica supported Co catalyst. The catalyst starts to reduce at about 500 ºC in H_2, with complete reduction only achievable at temperatures exceeding 800 ºC (**Figure 8a**). For CVD reaction performed in the temperature range of 500-700 ºC (**Figure 8b**), only a portion of Co^{2+} cations could be reduced to form Co nanoclusters, while the remaining Co^{2+} ions serve as anchoring sites, preventing the sintering of reduced Co particles, thus promoting the growth of small diameter SWNTs from CO carbon source, as schematically illustrated in **Figure 8c**[99].

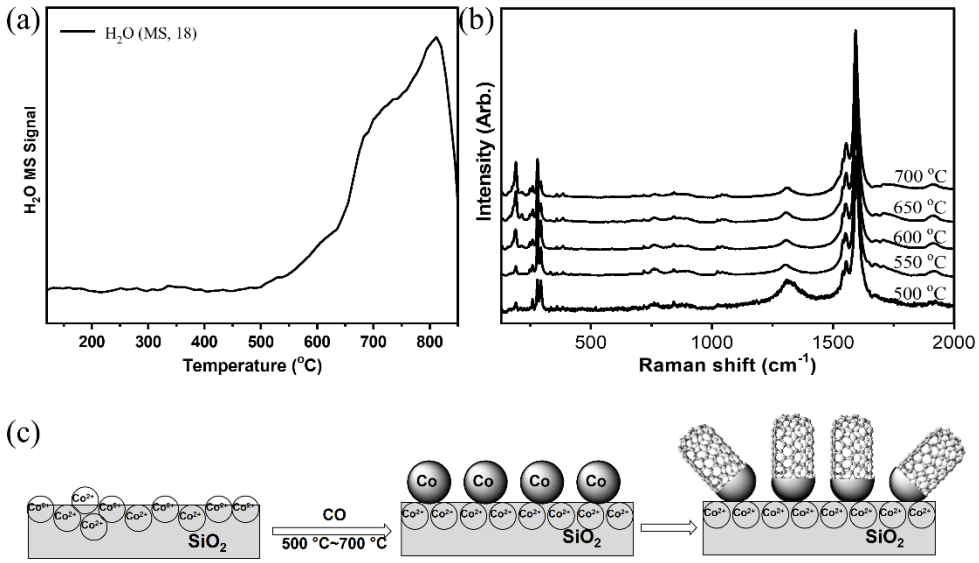

Figure 8. (a) H_2-TPR pattern of Co/SiO_2 catalyst prepared by ALD. (b) Raman spectra of SWNTs grown on Co/SiO_2 catalyst at various temperatures. (c) Schematic illustration of SWNT growth on a partially reduced Co/SiO_2 catalyst[99]. Copyright 2011 Royal Society of Chemistry

In addition to using unreduced Co^{2+} as anchors, reduced Co nanoparticles can be also stabilized on the support surface through regulating metal-support interactions. Due to their same crystal structures and similar lattice parameters, CoO could dissolve in the MgO matrix and form an ideal $Co_xMg_{1-x}O$ solid solution after annealing at 1000 °C for 20 h[103], as revealed by the uniform face-centered cubic (200) lattice fringes of single crystal structure (**Figure 9a**). Using in situ ETEM, the reduction of surface Co^{2+} upon CO reduction was monitored at 600 °C. **Figure 9b** presents a TEM image of homogeneous Co nanoparticles formed on the MgO surface. The calculated fast Fourier transformation (FFT) pattern (**Figure 9c**) exhibits an epitaxial relationship between the Co nanoparticles and the MgO support. Lattice-mismatched epitaxy was also confirmed by a zoomed-in view of a Co nanoparticle (**Figure 9d**). Owing to the significant lattice constant mismatch between the Co and MgO (~16%), the misfit strain at the Co/MgO interface causes apparent deformation of the Co lattice, which minimizes the interface area and limits the formation of large diameter Co nanoparticles. The epitaxially formed Co nanoparticles not only exhibit uniform size and crystal structure, but also are well anchored by the underlying MgO support. Consequently, the $Co_xMg_{1-x}O$ solid solution affords the predominant growth of (6, 5) SWNTs using CO CVD at 500 °C (**Figure 9e-f**). For comparison, SWNTs grown from an ALD prepared MgO supported Co catalyst, which does not exhibit such metal-support epitaxy under reaction conditions, display a much wider chirality distribution[104].

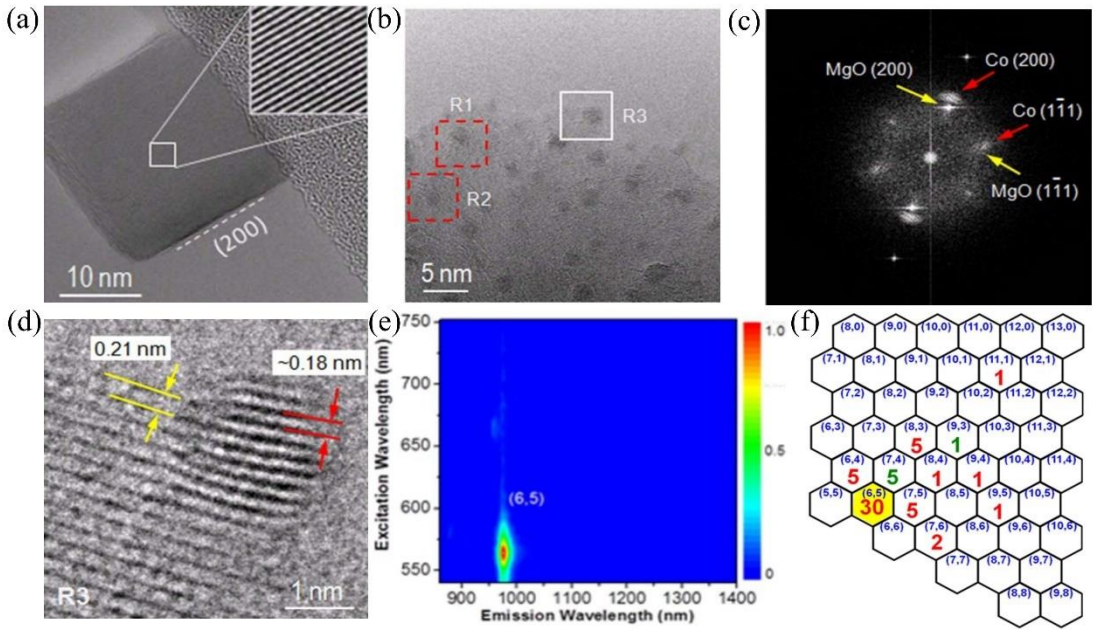

Figure 9. (a) TEM image of a representative cube particle of the $Co_xMg_{1-x}O$ catalyst. (b) An *in situ* HRTEM lattice image of Co nanoparticles formed from reducing the $Co_xMg_{1-x}O$ solid solution and (c) the calculated FFT digital diffractogram. (d) Atomic arrangement of the epitaxial structure. A high chiral selectivity growth of (6, 5) nanotubes determined by (e) PL and (f) nanobeam electron diffraction[103]. Copyright 2013 Nature Publishing Group

However, the epitaxy between Co and the MgO support could be destroyed when increasing the reaction temperature to 700 ºC[53], where severe particle coalescence occurs. An alternative strategy to stabilize the supported Co catalyst involves using a support material with abundant anchoring sites. For example, Wu et al.[61] prepared an MgO supported Co catalyst that was mildly annealed at 450 ºC for 1 h prior to use. The surface of the mildly treated MgO contains many vacancies, such as the vacancies arising from the lack of O^{2-} and the neutral vacancy site, which possess unsaturated valence and a large electron affinity. These characteristics tend to promote ionization and stabilize the reduced Co nanoparticle. As a result, the supported Co nanoparticles are well anchored on the surface and can resist sintering even at 800 ºC. Using ambient CO CVD, preferential synthesis of (6, 5) or (7, 5) SWNTs was respectively realized at 700 ºC and 800 ºC (**Figure 10**).

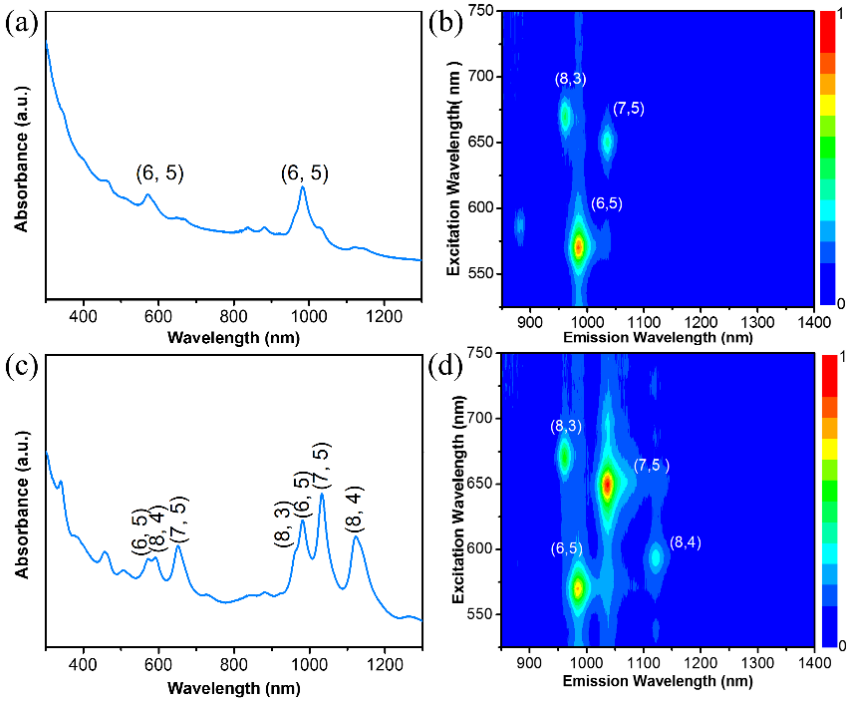

Figure 10. (a) UV-vis-NIR absorption spectrum and (b) PL emission map of SWNTs synthesized at 700 °C. (c) UV-vis-NIR absorption spectrum and (d) PL emission map of SWNTs synthesized at 800 °C[61]. Copyright 2022 Elsevier

In contrast to the common growth of (6, 5), (7, 5) and (7, 6) SWNTs with small diameters, selective growth of (9, 8) SWNTs was reported by Chen's group[105-107]. In their work, a mesoporous silica matrix, named TUD-1 was chosen as the support, and 1 wt% Co was incorporated at tetrahedral sites of the silica matrix using a hydrothermal approach[105]. The catalyst was initially reduced in 1 bar H_2 at 500 °C for 1 h, and CVD growth was performed at 800 °C using high pressure CO as the carbon precursor. **Figure 11a** shows the PL map of SWNTs sonicated in a sodium dodecyl benzene sulfonate D_2O solution. Grounded on PL emission intensities, the selectivity of (9, 8) SWNTs was calculated to be about 59.1% among the semiconducting nanotubes. The prereduction temperature was revealed to be crucial in selectively growing (9, 8) nanotubes of 1.17 nm. **Figure 11b** compares UV-vis-NIR absorption of SWNTs synthesized from the Co-TUD-1 catalyst pre-reduced at different temperatures. At a lower reduction temperature (400 °C), there is less reduced Co atoms, leading to the formation of small diameter Co nanoparticles for growing small diameter (6, 5) SWNTs. On the contrary, a higher reduction temperature (600 °C) causes the formation of nanoparticles with different sizes, leading to a loss of control over the SWNT (n, m) selectivity. Later, Wang et al.[106] designed a sulfate-promoted $CoSO_4/SiO_2$ catalyst, which exhibited a narrow H_2 reduction peak at 470 °C, for selectively growing (9, 8) SWNTs (**Figure 11c**). After reduction at 540 °C in H_2, the highly dispersed $CoSO_4$ evolved into uniform Co nanoparticles with an average diameter 1.23 nm, matching the diameter of (9, 8) nanotube. Catalysts reduced under different conditions exhibited different sulfur content, correlated with the change in (n, m) selectivity. The presence of sulfur in the catalyst could inhibit the aggregation of Co atoms by forming Co-S compounds, which demonstrates the potential of tuning SWNT chirality distribution by promoting the catalyst with a main group element.

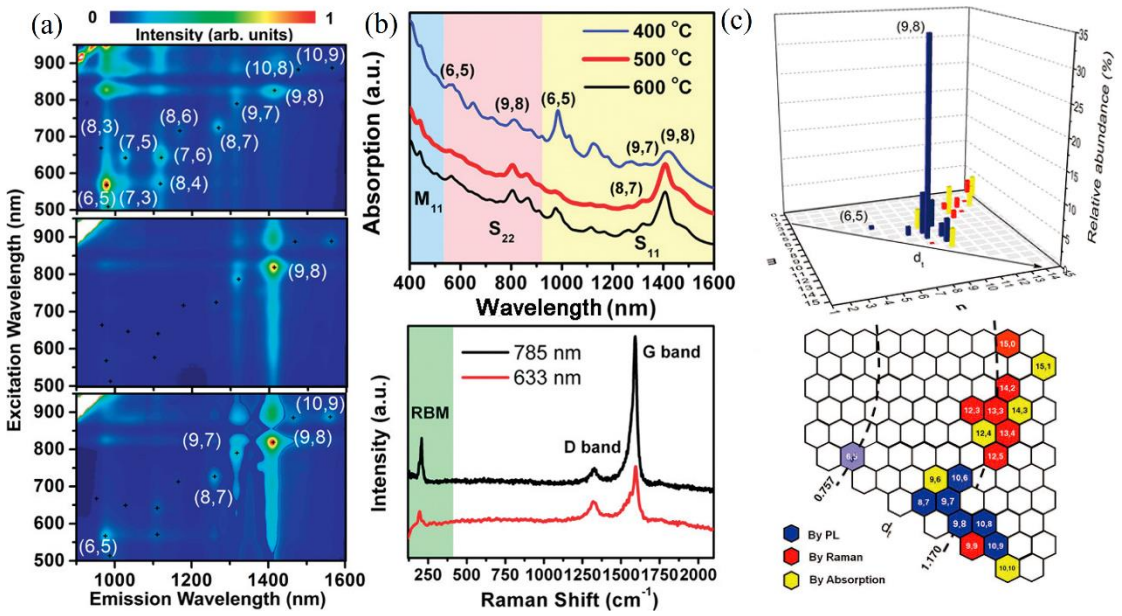

Figure 11. (a) PL emission map of SWNTs synthesized from Co-TUD-1 catalyst at different temperatures. (b) UV-vis-NIR spectra and Raman spectra of as-synthesized SWNTs[105]. Copyright 2010 American Chemical Society. (c) Relative abundance of (n, m) SWNTs produced from the $CoSO_4/SiO_2$ catalyst and two-dimensional projected chirality map of SWNTs[106]. Copyright 2012 American Chemical Society

In addition to main group element, other transition metals, like Cr and Mn, have been added into Co-containing heterogeneous catalysts to enable the growth of SWNTs with narrow (n, m) distributions[108, 109]. In 2009, Loebick et al.[109] studied the growth of SWNTs using Cr-promoted Co-MCM-41 catalysts with varying Co:Cr atomic ratios. **Figure 12a-c** shows the contour plot of normalized PL spectra intensities for SWNTs grown on the monometallic Co catalyst, bimetallic CoCr with 3:1, and 1:1 ratios. The most abundant species in all the products were (6, 5), (7, 5) and (7, 6). With an increasing proportion of Cr, the relative abundance of small diameter (6, 5) increased. The shift in (n, m) was correlated with the development of oxide in the MCM-41 framework. The less reducible chromium oxide not only influenced the reducibility of the cobalt ions, but also aided in anchoring reduced Co clusters for engineering the SWNT diameters. Later, the authors reported the selective growth of subnanometer semiconducting SWNTs from an MCM-41 silica supported CoMn bimetallic catalyst with a Co: Mn molar ratio of 1:3[56]. TEM characterizations revealed that most of SWNTs synthesized at 600 °C fell within the diameter range of 0.5-0.7 nm. By combining PL and Raman characterizations, they

concluded that semiconducting SWNTs (93%) were favored to grow at such a low reaction temperature (**Figure 12d**). From the catalyst perspective, the size and shape of the catalyst particles played a role in enriching semiconducting nanotubes.

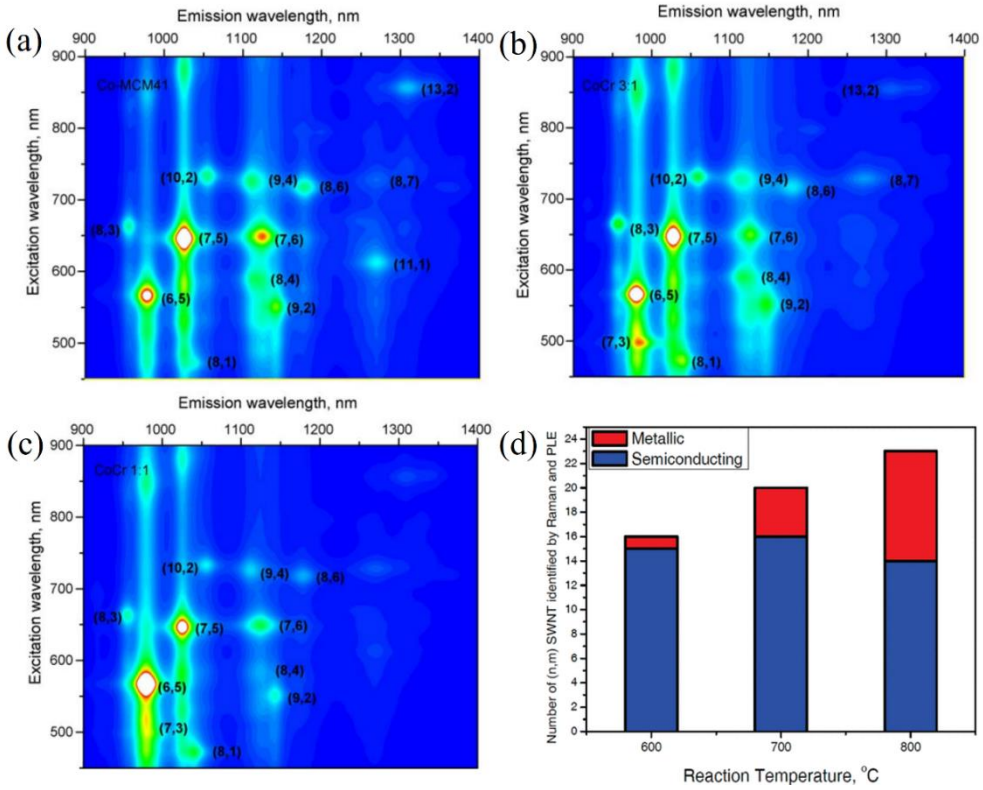

Figure 12. (a-c) PL emission map of SWNTs grown on the monometallic Co catalyst, bimetallic CoCr 3:1, and 1:1 catalyst, respectively[109]. Copyright 2009 Elsevier. (d) Number of metallic and semiconducting sub-nanometer SWNTs as determined by (n, m) indices[56]. Copyright 2010 American Chemical Society

Without adding promoters, it is also possible to modify the chirality distribution of SWNTs. In 2017, Xu et al.[66] proposed to control the SWNT chirality by tuning the oxidation degree of a zeolite supported Co catalyst. Using plasma CVD with CH_4 as the carbon feed, dominant synthesis of (6, 5) SWNTs was achieved on a non-pretreated catalyst. However, the catalyst was pretreated with optimized contents of N_2, H_2 and H_2O at temperatures over 700 °C, leading to controlled surface oxidation of Co nanoparticles, which catalyzed the selective growth of (6, 4) tube with a concentration up to 57%. First-principles calculations demonstrated that the surface oxidation degree affected the binding energies of nanotube cap and edge on the catalyst surface, thus driving the formation of SWNTs with smaller diameter and larger chiral angle. This work provides another promising strategy for regulating SWNT chirality distribution when using solid supported Co as the catalyst.

4.2.2 *Fe-based catalysts*

Similar to Co catalysts, solid supported Fe catalysts have also aroused significant interests in selectively growing SWNTs due to their cost-effectiveness. Although Li et al. reported the highly efficient growth of SWNTs from MgO supported Fe catalyst as early as 2001[45], the efficiency of monometallic Fe catalysts in synthesizing SWNTs at low reaction temperatures, which are preferred for achieving a narrow chirality distribution, has been limited. This is because the complete reduction of supported iron oxide, which takes place gradually from Fe_2O_3 to Fe_4O_3, FeO and Fe(0), can only be achieved at temperatures exceeding 700 °C. As a result, at reaction temperatures below 700 °C, only a trace amount of large diameter iron oxide nanoparticles, which have weak interactions with the underlying oxide support, could be activated for growing mainly multi-walled carbon nanotubes[37]. While SWNTs can be grown on monometallic Fe catalyst at temperatures higher than 700 °C, the products usually exhibit a relatively wide diameter distribution. In a study conducted by Ago et al.[110] in 2005, they studied chirality distribution of SWNTs synthesized by CH_4 CVD over MgO supported Fe catalyst at 750 °C. **Figure 13a** presents Raman spectra of SWNTs grown from catalysts with varying Fe loadings. At a 3 wt% Fe loading in the catalyst, the strongest RBM was centered at 182 cm^{-1}, which corresponds to SWNTs with diameter

of 1.32 nm. Decreasing the Fe loading to 0.6 wt% shifted the strongest RBM peaks to a higher frequency of 265 cm^{-1}, corresponding to 0.9 nm SWNTs. A further decrease in Fe content resulted in no SWNT growth, suggesting that the Fe concentration was too low to form viable particles. The absorption and PL spectra of SWNTs grown from 0.6 wt% Fe loading confirmed that SWNTs with diameters close to 0.9 nm, such as (7, 5) and (7, 6) nanotubes, were the major species in the product (**Figure 13b-c**). However, the use of CH_4 as carbon source led to the presence of various (n, m) species in the product. Using CO as the carbon precursor, an ALD prepared Fe/MgO catalyst afforded the synthesis of SWNTs with a relatively narrow (n, m) distribution[62]. **Figure 13d** compares the Raman spectra of SWNTs grown on the Fe/MgO catalyst at 700 °C and 800 °C. Obviously, mainly high frequency RBMs were observed for the SWNTs grown at 700 °C, indicating the preferential synthesis of small diameter SWNTs. The PL emission intensity map verified the dominance of (6, 5) nanotubes (**Figure 13e**). The schematic illustration of Fe catalyst activation and carbon nanotube growth on the MgO supported monometallic Fe catalyst is presented in **Figure 13f**.

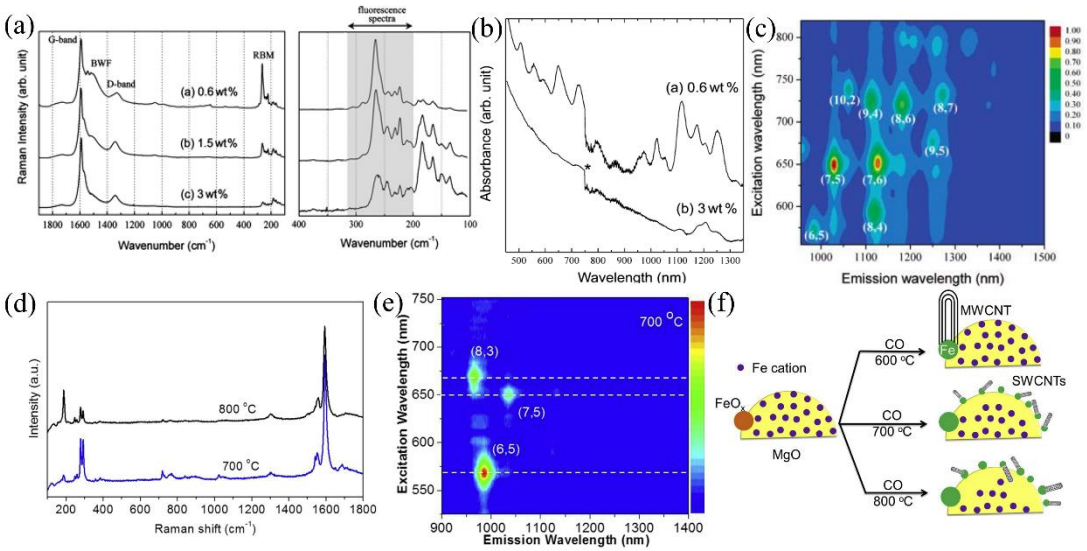

Figure 13. (a) Raman spectra of SWNTs grown from catalysts with different Fe loadings. (b-c) UV-vis-NIR spectra and PL emission map of SWNTs grown from 0.6 wt% Fe loading[110]. Copyright 2005 American Chemical Society. (d) Raman spectra of carbon nanotubes grown on Fe/MgO catalyst by CO CVD. (e) PL emission map of SWNTs synthesized on Fe/MgO catalyst at 700 °C. (f) Schematic illustration of carbon nanotube growth at different reaction temperatures on Fe/MgO catalyst[62]. Copyright 2016 Elsevier

To achieve a narrower SWNT chirality distribution while operating at lower reaction temperatures, numerous strategies have been explored over the past two decades to enhance the reducibility and activating supported iron oxide. One commonly employed approach involves introducing a second metal, such as Ru[57], Cu[37, 58], or Mn[62], to promote the low temperature reduction of iron oxide. In 2007, Li et al.[57] reported a silica supported FeRu catalyst for CH_4 CVD growth of SWNTs. Owing to the presence of Ru, the bimetallic catalyst predominantly grows (6, 5) SWNTs at 600 °C, which was attributed to the low eutectic temperature of Fe and Ru. The intimate alloying of FeRu affords the formation of small diameter catalyst particles that resist high temperature sintering, consequently catalyzing the growth of small diameter SWNTs. Compared with CoMoCAT (6, 5) SWNTs, the FeRu-grown SWNTs exhibit a similarly narrow chirality distribution. Even narrower (n, m) distribution and higher selectivity to (6, 5) SWNTs were achieved on an MgO supported FeCu catalyst[37]. In the catalyst system, CuO is readily reduced at 600 °C in the presence of CO, aiding in the reduction of adjacent iron oxide through a "spillover" mechanism. As a result, small diameter FeO_x particles are reduced with the assistance of Cu, enabling low temperature growth of SWNTs. Compared with previously reported (6, 5) SWNTs[55, 57], this approach exhibited significantly higher selectivity to (6, 5) tube, as confirmed through nanobeam electron diffraction characterizations of individual SWNTs[58]. Two key factors contribute to this narrow chirality distribution. One is the use of CO, which demonstrates a high carburization potential for metal nanoparticle carburization. The other is the high carbon solubility of Fe[68, 111], which facilitates the growth of SWNTs with diameters much smaller than the catalyst particle.

Building upon the insights mentioned above, an MgO supported FeMn catalyst was developed for chiral selective growth of SWNTs[62]. In comparison to the H_2-TPR profiles of monometallic Fe and Mn, the presence of Mn significantly enhances the reducibility of Fe. Like other catalysts designed for low-temperature growth[57, 58, 60, 99], the FeMn catalyst produced mainly (6, 5) SWNTs at 600 °C by CO CVD, where the synergistic effects

between Fe and Mn come into play. Moreover, the chirality distribution of SWNTs grown at 800 °C is comparable to that of nanotubes synthesized on monometallic Fe catalyst, indicating that the role of Mn is primarily to facilitate the dispersion and reduction of the Fe catalyst, with minimal impact on modifying the (n, m) distribution of synthesized SWNTs.

In addition to regulating the metal composition, it is possible to enhance the reducibility of FeO_x by using composite supports[112, 113]. In 2022, Han et al.[112] reported the growth of SWNTs using a porous MgO promoted Fe/SiC catalyst at 650 °C. SiC with high thermal conductivity, preventing the formation of local hot spots during the reaction, serves as a catalyst support. However, SiC support Fe catalyst alone could not grow SWNTs by CO CVD at 850 °C. The H_2-TPR profile of the Fe/SiC catalyst reveals that FeO_x is difficult to reduce, possibly due to the covering of Si_xO_y layer that induces a strong iron oxide-support interaction. In contrast, when the Fe/SiC catalyst is mixed with porous MgO, it can be activated for growing SWNTs. **Figure 14a** depicts the Raman spectra of carbon nanotubes grown on the MgO promoted Fe/SiC catalyst at different temperatures. Clearly, SWNTs could be grown at a reaction temperature as low as 650 °C. The success in growing SWNTs at low temperatures is reflected by the H_2-TPR patten of the promoted catalyst (**Figure 14b**). Due to the presence of MgO, the Fe/SiC catalyst could be effectively reduced at temperatures below 650 °C, corresponding to the catalyst's activation at 650 °C. Remarkably, Raman spectra of SWNTs grown at 650 °C only exhibit RBMs with frequencies higher than 280 cm^{-1}, indicating the formation of SWNTs thinner than 0.9 nm. UV-vis-NIR absorption spectroscopy (**Figure 14c**) and PL spectroscopy (**Figure 14d**) characterizations suggest the SWNTs possess a very narrow chirality distribution with highly enriched (6, 5) tubes, even comparable to those grown from FeCu/MgO[37] and FeRu/SiO_2[57] catalysts. The high chirality selection is attributed to the high thermal conductivity of SiC, which minimizes the temperature difference between different regions in the catalyst during the growth process. Furthermore, the active composition of Fe and the use of CO carbon precursor are of equally importance in determining such an (n, m) distribution. This work introduces a novel strategy for activating catalyst particles and provides guidance for designing oxide promoted heterogeneous catalysts for chiral-selective growth of SWNTs.

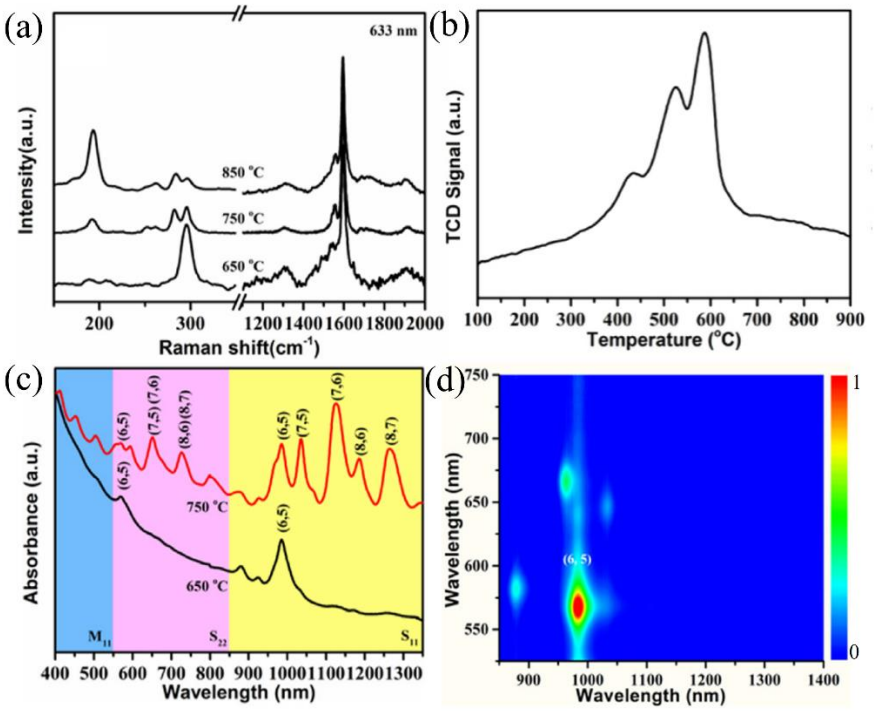

Figure 14. (a) Raman spectra of SWNTs grown at different temperatures from Fe/SiC catalyst. (b) H_2-TPR pattern of MgO promoted Fe/SiC catalyst. (c) UV-vis-NIR absorption spectra of dispersed SWNTs grown at 650 °C and 750 °C. (d) PL emission map of SWNTs synthesized at 650 °C[112]. Copyright 2022 Elsevier

4.2.3 *Ni-based catalysts*

Compared with extensive studies on solid supported monometallic Co or Fe catalysts for CVD growth of SWNTs, there is a scarcity of reports on the development of supported Ni catalysts. In 2005, Yang et al.[114] reported the preparation of highly ordered Ni-MCM-41 with nearly atomically dispersed nickel ions using a

hydrothermal method. By varying the chain length of the surfactant, the porosity and pore size could be well controlled. Similar to the Co-MCM-41 catalyst[98], the Ni-MCM-41 catalyst was physically stable at high reaction temperatures and afforded the growth of SWNTs through CO disproportionation. Although it had a lower reduction temperature than Co-MCM-41, detailed investigations of SWNTs grown from the Ni-MCM-41 catalyst were lacking in the work. Taking the advantage of the easy reduction of monometallic Ni catalyst, Chiang et al.[115] reported gas phase formation of SWNTs using Ni catalyst introduced from a micro-plasma reactor. However, the prepared SWNTs from gas phase demonstrated a broad chirality distribution, with the 0.9 nm (7, 6) and (9, 4) tubes exhibiting the strongest PL emission intensities.

In 2012, He et al.[60] designed a silica supported Ni catalyst (Ni/SiO_2) using ALD technique for the low temperature growth of SWNTs. H_2-TPR profile revealed that the catalyst began reducing at 400 °C and the reduction continued until exceeding 700 °C (**Figure 15a**). This behavior suggested the possible formation of Ni_2SiO_4 during catalyst preparation process. CO CVD growth of carbon nanotubes was tested in the temperature range of 450-800 °C. **Figure 15b** presents the Raman spectra of SWNTs grown at different temperatures. RBMs were observed from the Raman spectra acquired from the samples grown at 450 °C, although the quality and purity of SWNTs were poor, as indicated by the relatively large D mode intensity. High quality SWNTs were successfully synthesized at a temperature as low as 500 °C. The intensity ratio between G to D mode was about 28, comparable to that of SWNTs grown at 800 °C. **Figure 15c** shows the PL map of the dispersion of SWNTs grown at 500 °C, which demonstrates that (6, 5) SWNTs are the major species in the products, even though the chirality distribution is not as narrow as those grown from Fe catalyst[45, 110]. This could be attributed to the lower carbon solubility of Ni than Fe. During the CVD process, the Ni catalyst is partially reduced, and the unreduced Ni^{2+} species constrain the mobility of reduced Ni nanoparticles, facilitating the formation of small diameter Ni nanoparticles for growing small diameter SWNTs[60]. This work paves the way towards low temperature growth of SWNTs using supported Ni catalyst.

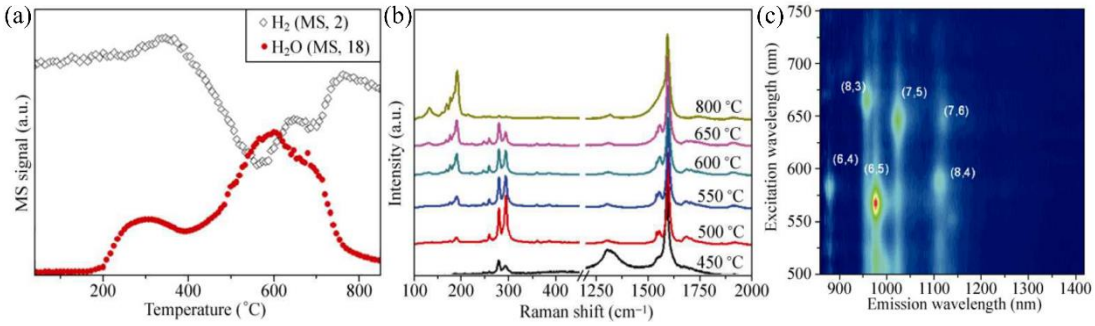

Figure 15. (a) H_2-TPR pattern of the Ni/SiO_2 catalyst. (b) Raman spectra of carbon nanotubes grown on a Ni/SiO_2 catalyst at different temperatures. (c) PL emission map of SWNTs grown on a Ni/SiO_2 catalyst[60]. Copyright 2010 Tsinghua University Press and Springer-Verlag Berlin Heidelberg

To gain a deeper understanding of the metal particle anchoring mechanism and to improve the SWNT chirality selectivity, an MgO supported Ni catalyst (Ni/MgO) was developed for the low temperature growth of SWNTs[116]. Similar to CoO, NiO also shares a similar lattice parameter as MgO, thus favoring the formation of uniform solid solution upon calcination. The authors studied the effect of catalyst calcination temperature on the performance of Ni/MgO catalyst. Catalyst heated at a low temperature of 450 °C resulted in supported Ni predominantly existing as unreacted and surface NiO. These species had weak interaction with the underlying MgO surface, and were prone to aggregation, forming large Ni particles under reaction conditions, which were unfavorable for the growth of SWNTs. Conversely, Ni/MgO calcined at a high temperature of 800 °C caused the migration of Ni^{2+} into the MgO matrix and difficulty in Ni^{2+} reduction. Consequently, only a small amount of SWNTs were produced from the 800 °C-annealed catalyst by CO CVD. The optimized calcination temperature was determined to be 600 °C, at which enriched (6, 5) tubes were obtained at a CVD reaction temperature of 600 °C. Using DFT calculations, the binding energies between reduced Ni(0) and the support were calculated[116]. The results revealed that the presence of underlying Ni^{2+} significantly enhanced the binding energy between Ni(0) and the support. The anchoring effect of subsurface Ni^{2+}, the use of CO carbon precursor, and the low reaction temperature collectively contributed to the narrow chirality distribution of Ni-grown SWNTs. This work highlights the importance of anchoring effect in achieving chiral-selective growth of SWNTs.

4.2.4 *Mixed metal catalysts*

Different from bimetallic catalyst systems where only one element is actively involved in SWNT growth, the mixed catalyst category defined here encompasses a class of catalyst in which at least two different metals can independently catalyze SWNT growth or form alloy nanoparticles that participate in the process. An illustrative example of this is a zeolite supported FeCo catalyst, which is employed as the catalyst for alcohol CVD[52, 63, 117]. The binary phase diagram of FeCo suggests that no alloy phase forms under the reaction conditions. Consequently, it is hypothesized that a synergistic effect occurs in which the activities of both the Fe and Co nanoparticles are enhanced when using such mixed metal catalysts.

In 2022, Hao et al. developed an FeCo/layered double hydroxide (LDH) catalyst for selectively growing subnanometer SWNTs [118]. The LDHs containing mixed metals were prepared by a coprecipitation technique, and the molar ratio of Fe: Co: Mg: Al was 0.2:0.2:2:1. Before CVD growth, the catalyst underwent annealing at 1000 °C for 6 h. **Figure 16a** shows the XRD pattern of the prepared catalyst. Except for diffraction peaks corresponding to MgO and $MgAl_2O_4$, peaks assigned to iron oxide or cobalt oxide were not detected, indicating the well dispersion of Fe and Co. Compared with monometallic Fe/LDHs, the FeCo/LDH catalyst allowed for the synthesis of SWNTs with a narrower chirality distribution and enriched (6, 5) nanotubes at a lower reaction temperature (**Figure 16b**). Moreover, the SWNT density grown from the mixed metal catalyst was much higher than that grown from Fe/LDHs[118], highlighting the importance of the synergistic effect in selectively growing SWNTs. This research extends the applications of LDH supported mixed metals for synthesizing SWNTs with a narrowly distributed chirality distribution.

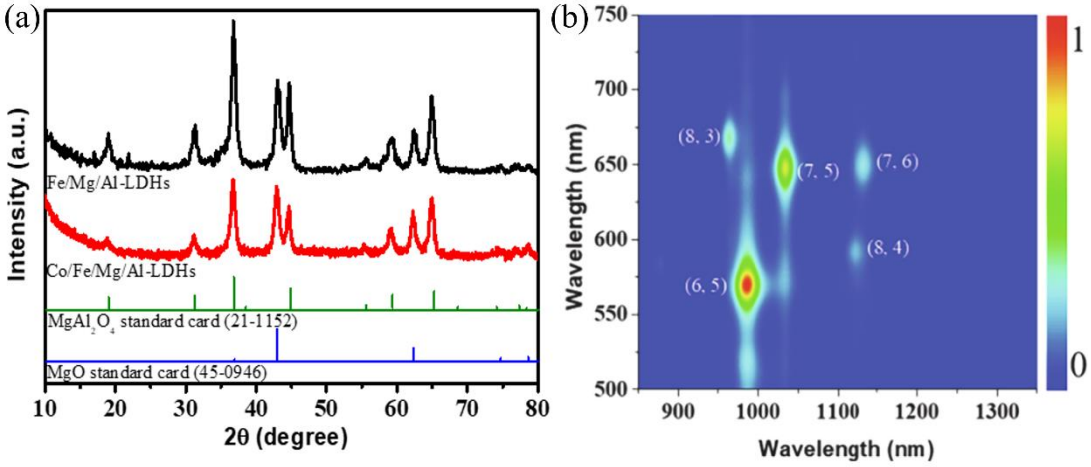

Figure 16. (a) XRD pattern of FeMgAl/LDHs. (b) PL emission map of SWNTs grown from on FeMgAl/LDHs at 700 °C[118]. Copyright 2022 Elsevier

4.3 *Noble metal catalysts*

The catalytic performance of supported metal catalyst is sensitive to the electron filling state of the outmost *d* orbits[119-121], which governs the carbon source absorption and dissociation. Noble metals, typically having a high electron filling degree in their *d* orbits, are not very active for growing SWNTs. Although almost all metals have been demonstrated to be capable of growing SWNTs on flat surfaces[95, 122], such as quartz and sapphire, the poor yield of the surface-grown SWNTs hinderers their systematic investigations. The yield limitation makes it challenging to establish a direct link between the catalyst element and SWNT chirality distribution.

Aiming at the bulk synthesis of SWNTs from noble metal catalysts, Zhang et al.[123] introduced an MgO supported Ru catalyst for growing SWNTs with CO as the carbon precursor. The Ru/MgO prepared by impregnation exhibited atomically dispersed Ru on the porous MgO support. Upon exposure to CO at reaction temperatures, Ru atoms were reduced and migrated to form small Ru clusters, which subsequently catalyzed the growth of SWNTs. The bulk synthesis of SWNTs was achieved through the activation of Ru nanoparticles, which was addressed with the assistance of DFT calculations. **Figure 17a** indicates that the Ru activation begins with CO absorption and dissociation. On a free Ru_8 cluster, CO molecules absorb weakly (0.4 eV) and can easily desorb. Furthermore, the dissociation barrier for CO on the free Ru_8 cluster is too high (2.6 eV) to be overcome during the CVD reaction process (**Figure 17b**). The calculation results are consistent with previous report that Ru, located out of the Goldilocks zone and is unsuitable for SWNT growth[104]. However, an MgO supported Ru_8 cluster exhibited superior CO dissociation properties. The electronic structure analysis revealed orbital hybridization between the *d* orbitals of Ru atoms and the *p* orbitals of O atoms in MgO, indicating electron transfer from MgO

to Ru_8 (**Figure 17c**). The excessive electrons of Ru_8 are donated from the *d* orbits to the antibonding π^* molecular orbits of CO molecules, thus enhancing the absorption and dissociation of CO (**Figure 17d**), and moving the supported Ru catalyst into the "Goldilocks zone" for SWNT synthesis. The activation mechanisms were also found to be applicable to MgO supported Re and Pd catalysts[124, 125]. Similar DFT calculations revealed that electron accumulation at Pd/MgO interface upshifted the *d* band center of Pd towards to the Fermi energy, leading to a strong metal-carbon interaction and the activation of the MgO supported Pd catalyst.

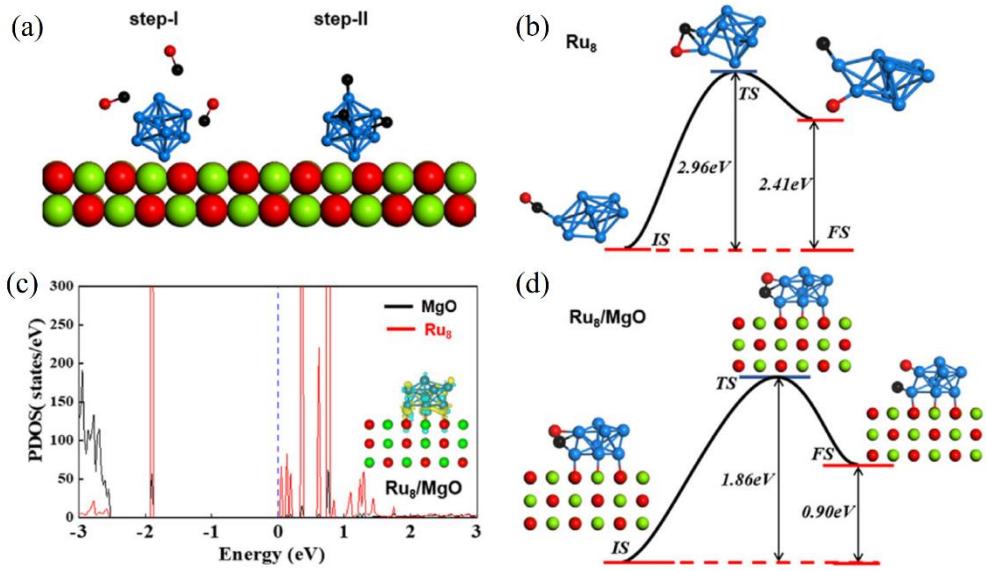

Figure 17. (a) Schematic diagram of the CO dissociation processes on Ru_8/MgO. Energy profile of the dissociation processes of CO on (b) free Ru_8 and (d) Ru_8/MgO. (c) Partial density of states of Ru_8/MgO. Inset is the charge density difference plot of Ru_8/MgO[123]. Copyright 2022 Elsevier

The (n, m) distributions of SWNTs synthesized on various MgO supported noble metals were presented in **Figure 18**[123-125]. It was observed that the Ru catalyst allowed for the preferential synthesis of (6, 5) nanotubes even at a high reaction temperature of 850 °C. Additionally, other small-diameter SWNTs, such as (6, 4), (8, 3), (7, 5), and (8, 4), were found to be less abundant in the Ru-grown SWNTs. The chirality distribution in Ru-catalyzed SWNTs was similar to those grown on Fe-family metals, with larger chiral angle SWNTs typically being enriched[126]. Notably, supported noble metal catalysts typically require higher reaction temperatures for activation. For instance, the lowest temperature for SWNT growth from MgO supported Re catalyst was 800 °C[124]. This higher reaction temperature led to a wide chirality distribution. However, the yield of SWNTs grown on the catalyst was high enough to enable subsequent separation based on diameters using gel chromatography. SWNTs with diameter ranges of 0.65-1.1 nm and 1.1-1.7 nm were successfully separated, offering potential applications in various fields where SWNT diameter matters. In contrast, the threshold for SWNT synthesis on an MgO supported Pd catalyst was even higher, requiring temperatures greater than 900 °C[125]. In the products, near armchair and (2n, n) nanotubes were enriched, a result attributed to SWNT growth kinetics and the interfacial energy between the metal catalyst and SWNTs[38]. These studies shed light on bulk synthesis of SWNTs using supported noble metals, and the chemical composition and crystal structure of the catalysts may hold the key to achieving enriched SWNTs with specific (n, m) chirality.

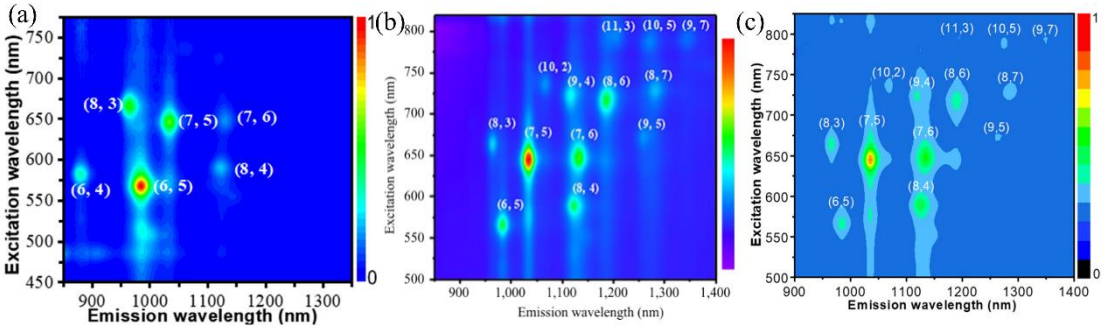

Figure 18. PL emission map of SWNTs grown from (a) Ru/MgO catalyst at 850 ºC, (b) Re/MgO catalyst at 800 ºC, and (c) Pd/MgO catalyst at 900 °C[123-125]. Figure (a) adapted with permission from ref [123]. Copyright 2022 Elsevier. Figure (b) adapted from ref [124] Copyright 2022 Tsinghua Press. Figure (c) adapted with permission from ref [125]. Copyright Springer-Verlag GmbH

5. Challenges and Prospects

Indeed, the scientific community has made significant strides in the chiral-selective growth of SWNTs. However, there remain many challenges in the field of SWNT synthesis. Some of these challenges include:

1. Understanding Catalyst Behavior: The connections between SWNT chirality distribution and heterogeneous catalyst have not been firmly established. Catalyst performance is highly sensitive to the catalyst preparation procedure, and even minor change can lead to significant variations in catalytic behaviors and SWNT growth outcomes. Therefore, a deeper understanding of the catalytic mechanisms is required, relying on more in situ characterization techniques and theoretical calculations.

2. Diversifying Catalysts: While certain supported noble metals have been developed for synthesizing SWNTs, the range of supported metal catalysts is still limited compared to the metal catalysts used in surface growth of SWNTs. More efforts should be directed towards designing and developing supported metal catalysts beyond those that already existed.

3. High-Temperature Growth: Achieving narrow SWNT chirality distributions is typically feasible at relatively low reaction temperatures, but this might result in synthesized SWNTs with a lower degree of graphitization. Consequently, the challenge lies in how to selectively grow specific (n, m) SWNTs at high reaction temperatures. While catalysts with high melting temperatures have shown promise in surface growth of SWNTs, the SWNT growth window remains quite narrow. In the future, researches could focus on designing supported refractory catalysts for bulk growth of SWNTs.

4. Balancing Purity and Yield: The growth of high-purity SWNTs with specific (n, m) is often achieved at the expense of SWNT yield. In other words, only a very small proportion of catalyst particles is activated for growing SWNTs, while other particles that could potentially grow different nanotube species are deactivated intentionally. As a result, selectively grown SWNTs usually have a low yield. This issue might be addressed by designing industrial scale CVD reactors, which could comprise the low growth efficiency.

5. Sustainable Purification: The purification of SWNTs grown from heterogeneous catalysts is a crucial step before their application. Traditional methods often involve harsh acid treatments, which can lead to functionalization of SWNT surfaces. In the quest for more environmentally friendly processes, there is a growing demand for green purification methods that can effectively remove support materials and metal catalysts while preserving the pristine structure of SWNTs. Developing such green purification techniques is essential for ensuring the high quality and integrity of SWNTs for various applications.

6. Characterization Techniques: Developing more reliable techniques for characterizing SWNTs is indeed essential for advancing research in this field. While optical techniques and electron microscopy have been widely used to analyze SWNT products, each of these methods has its own set of advantages and limitations. A comprehensive approach that can provide detailed information about SWNT purity, quality, diameter, and chirality would be highly valuable. Establishing a standardized procedure for SWNT characterizations could significantly enhance the accuracy and consistency of research in this area.

7. Expanding Chirality Control: The selected SWNT chiralities achieved so far are mainly limited to (6, 5) or (9, 8) SWNTs with large chiral angles. Growing SWNTs with smaller chiral angles remains difficult. Although surface growth of (2n, n)[34, 35, 127] or near zigzag SWNTs[128, 129] with high purity has been reported, bulk synthesis of SWNTs with such chiralities have not been realized. To fully harness the extraordinary properties of SWNTs with specific (n, m), further efforts are needed to optimize both supported catalyst and CVD reaction parameters.

The prospects for SWNT applications are intricately tied to the quality and quantity of the SWNT materials. Achieving bulk synthesis of SWNTs with narrow chirality distributions using heterogeneous catalysts is crucial for providing a sufficient supply of materials for their potential cutting-edge applications. Coupled with recent advancements in chirality separation[130, 131], ordered assembly[132], and high-performance field-effect transistor fabrication[133, 134], it is anticipated that we are on the cusp of a burgeoning era in SWNT-based technology. The potential for SWNTs to revolutionize various fields is promising, and ongoing research efforts are poised to unlock their full potential.

Acknowledgments

This work was supported by the Key Basic Research Project of Shandong Province (ZR2019ZD49), National Natural Science Foundation of China (51972184), and Taishan Scholar Foundation of Shandong Province (tstp20230627).

References

[1] Dresselhaus, M.; Dresselhaus, G.; Saito, R. Physics of carbon nanotubes. *Carbon* **1995**, *33*, 883–891, https://doi.org/10.1016/0008-6223(95)00017-8.
[2] He, M.; Zhang, S.; Zhang, J. Horizontal Single-Walled Carbon Nanotube Arrays: Controlled Synthesis, Characterizations, and Applications. *Chem. Rev.* **2020**, *120*, 12592–12684, https://doi.org/10.1021/acs.chemrev.0c00395.
[3] He, M.; Dong, J.; Zhang, K.; Ding, F.; Jiang, H.; Loiseau, A.; Lehtonen, J.; Kauppinen, E.I. Precise Determination of the Threshold Diameter for a Single-Walled Carbon Nanotube To Collapse. *ACS Nano* **2014**, *8*, 9657–9663, https://doi.org/10.1021/nn5042812.
[4] Bronikowski, M.J.; Willis, P.A.; Colbert, D.T.; Smith, K.A.; Smalley, R.E. Gas-phase production of carbon single-walled nanotubes from carbon monoxide via the HiPco process: A parametric study. *J. Vac. Sci. Technol. A* **2001**, *19*, 1800–1805, https://doi.org/10.1116/1.1380721.
[5] Dresselhaus, M.S.; Dresselhaus, G.; Saito, R.; Jorio, A. Raman spectroscopy of carbon nanotubes. *Phys. Rep.* **2005**, *409*, 47–99, https://doi.org/10.1016/j.physrep.2004.10.006.
[6] Peng, L.-M.; Zhang, Z.; Qiu, C. Carbon nanotube digital electronics. *Nat. Electron.* **2019**, *2*, 499–505, https://doi.org/10.1038/s41928-019-0330-2.
[7] Sun, L.; Wang, X.; Wang, Y.; Zhang, Q. Roles of carbon nanotubes in novel energy storage devices. *Carbon* **2017**, *122*, 462–474, https://doi.org/10.1016/j.carbon.2017.07.006.
[8] Kong, J.; Franklin, N.R.; Zhou, C.; Chapline, M.G.; Peng, S.; Cho, K.; Dai, H. Nanotube Molecular Wires as Chemical Sensors. *Science* **2000**, *287*, 622–625, https://doi.org/10.1126/science.287.5453.622.
[9] Zhao, M.; Zhang, Q.; Jia, X.; Huang, J.; Zhang, Y.; Wei, F. Hierarchical Composites of Single/Double-Walled Carbon Nanotubes Interlinked Flakes from Direct Carbon Deposition on Layered Double Hydroxides. *Adv. Funct. Mater.* **2010**, *20*, 677–685, https://doi.org/10.1002/adfm.200901522.
[10] Iijima, S.; Ichihashi, T. Single-shell carbon nanotubes of 1-nm diameter. *Nature* **1993**, *363*, 603–605, https://doi.org/10.1038/363603a0.
[11] Bethune, D.S.; Kiang, C.H.; de Vries, M.S.; Gorman, G.; Savoy, R.; Vazquez, J.; Beyers, R. Cobalt-catalysed growth of carbon nanotubes with single-atomic-layer walls. *Nature* **1993**, *363*, 605–607, https://doi.org/10.1038/363605a0.
[12] Guo, T.; Nikolaev, P.; Thess, A.; Colbert, D.; Smalley, R. Catalytic growth of single-walled manotubes by laser vaporization. *Chem. Phys. Lett.* **1995**, *243*, 49–54, https://doi.org/10.1016/0009-2614(95)00825-o.
[13] Kong, J.; Soh, H.T.; Cassell, A.M.; Quate, C.F.; Dai, H. Synthesis of individual single-walled carbon nanotubes on patterned silicon wafers. *Nature* **1998**, *395*, 878–881, https://doi.org/10.1038/27632.
[14] He, M.; Zhang, S.; Wu, Q.; Xue, H.; Xin, B.; Wang, D.; Zhang, J. Designing Catalysts for Chirality-Selective Synthesis of Single-Walled Carbon Nanotubes: Past Success and Future Opportunity. *Adv. Mater.* **2018**, *31*, e1800805, https://doi.org/10.1002/adma.201800805.
[15] Y. Chen, J. Zhang, Chemical vapor deposition gowth of single-walled carbon nanotubes with controlled structures for nanodevice applications, Acc. Chem. Res. 47(8) (2014) 2273-2281.
[16] Terranova, M.L.; Sessa, V.; Rossi, M. The World of Carbon Nanotubes: An Overview of CVD Growth Methodologies. *Chem. Vap. Depos.* **2006**, *12*, 315–325, https://doi.org/10.1002/cvde.200600030.
[17] Reich, S.; Li, L.; Robertson, J. Control the chirality of carbon nanotubes by epitaxial growth. *Chem. Phys. Lett.* **2006**, *421*, 469–472, https://doi.org/10.1016/j.cplett.2006.01.110.
[18] Cheng, H.M.; Li, F.; Su, G.; Pan, H.Y.; He, L.L.; Sun, X.; Dresselhaus, M.S. Large-scale and low-cost synthesis of single-walled carbon nanotubes by the catalytic pyrolysis of hydrocarbons. *Appl. Phys. Lett.* **1998**, *72*, 3282–3284, https://doi.org/10.1063/1.121624.
[19] Nasibulin, A.G.; Moisala, A.; Brown, D.P.; Jiang, H.; Kauppinen, E.I. A novel aerosol method for single walled carbon nanotube synthesis. *Chem. Phys. Lett.* **2005**, *402*, 227–232, https://doi.org/10.1016/j.cplett.2004.12.040.
[20] Sun, D.; Timmermans, M.Y.; Tian, Y.; Nasibulin, A.G.; Kauppinen, E.I.; Kishimoto, S.; Mizutani, T.; Ohno, Y. Flexible high-performance carbon nanotube integrated circuits. *Nat. Nanotechnol.* **2011**, *6*, 156–161, https://doi.org/10.1038/nnano.2011.1.
[21] Chiang, I.W.; Brinson, B.E.; Huang, A.Y.; Willis, P.A.; Bronikowski, M.J.; Margrave, J.L.; Smalley, R.E.; Hauge, R.H. Purification and Characterization of Single-Wall Carbon Nanotubes (SWNTs)

Obtained from the Gas-Phase Decomposition of CO (HiPco Process). *J. Phys. Chem. B* **2001**, *105*, 8297–8301, https://doi.org/10.1021/jp0114891.
[22] Liao, Y.; Jiang, H.; Wei, N.; Laiho, P.; Zhang, Q.; Khan, S.A.; Kauppinen, E.I. Direct Synthesis of Colorful Single-Walled Carbon Nanotube Thin Films. *J. Am. Chem. Soc.* **2018**, *140*, 9797–9800, https://doi.org/10.1021/jacs.8b05151.
[23] Cheung, C.L.; Kurtz, A.; Park, H.; Lieber, C.M. Diameter-Controlled Synthesis of Carbon Nanotubes. *J. Phys. Chem. B* **2002**, *106*, 2429–2433, https://doi.org/10.1021/jp0142278.
[24] Hata, K.; Futaba, D.N.; Mizuno, K.; Namai, T.; Yumura, M.; Iijima, S. Water-Assisted Highly Efficient Synthesis of Impurity-Free Single-Walled Carbon Nanotubes. *Science* **2004**, *306*, 1362–1364, doi:10.1126/science.1104962.
[25] He, M.; Duan, X.; Wang, X.; Zhang, J.; Liu, Z.; Robinson, C. Iron Catalysts Reactivation for Efficient CVD Growth of SWNT with Base-growth Mode on Surface. *J. Phys. Chem. B* **2004**, *108*, 12665–12668, https://doi.org/10.1021/jp0489471.
[26] Maret, M.; Hostache, K.; Schouler, M.-C.; Marcus, B.; Roussel-Dherbey, F.; Albrecht, M.; Gadelle, P. Oriented growth of single-walled carbon nanotubes on a MgO(001) surface. *Carbon* **2007**, *45*, 180–187, https://doi.org/10.1016/j.carbon.2006.07.016.
[27] Han, S.; Liu, X.; Zhou, C. Template-Free Directional Growth of Single-Walled Carbon Nanotubes on a- and r-Plane Sapphire. *J. Am. Chem. Soc.* **2005**, *127*, 5294–5295, https://doi.org/10.1021/ja042544x.
[28] Zhang, Z.; Liang, X.; Wang, S.; Yao, K.; Hu, Y.; Zhu, Y.; Chen, Q.; Zhou, W.; Li, Y.; Yao, Y.; et al. Doping-Free Fabrication of Carbon Nanotube Based Ballistic CMOS Devices and Circuits. *Nano Lett.* **2007**, *7*, 3603–3607, https://doi.org/10.1021/nl0717107.
[29] Wang, J.; Jin, X.; Liu, Z.; Yu, G.; Ji, Q.; Wei, H.; Zhang, J.; Zhang, K.; Li, D.; Yuan, Z.; et al. Growing highly pure semiconducting carbon nanotubes by electrotwisting the helicity. *Nat. Catal.* **2018**, *1*, 326–331, https://doi.org/10.1038/s41929-018-0057-x.
[30] Hu, Y.; Kang, L.; Zhao, Q.; Zhong, H.; Zhang, S.; Yang, L.; Wang, Z.; Lin, J.; Li, Q.; Zhang, Z.; et al. Growth of high-density horizontally aligned SWNT arrays using Trojan catalysts. *Nat. Commun.* **2015**, *6*, 6099–6099, https://doi.org/10.1038/ncomms7099.
[31] Ismach, A.; Segev, L.; Wachtel, E.; Joselevich, E. Titelbild: Atomic-Step-Templated Formation of Single Wall Carbon Nanotube Patterns (Angew. Chem. 45/2004). *Angew. Chem.* **2004**, *116*, 6135–6135, https://doi.org/10.1002/ange.200490155.
[32] Huang, S.; Cai, X.; Liu, J. Growth of Millimeter-Long and Horizontally Aligned Single-Walled Carbon Nanotubes on Flat Substrates. *J. Am. Chem. Soc.* **2003**, *125*, 5636–5637.
[33] Jin, Z.; Chu, H.; Wang, J.; Hong, J.; Tan, W.; Li, Y. Ultralow Feeding Gas Flow Guiding Growth of Large-Scale Horizontally Aligned Single-Walled Carbon Nanotube Arrays. *Nano Lett.* **2007**, *7*, 2073–2079, https://doi.org/10.1021/nl070980m.
[34] Yang, F.; Wang, X.; Zhang, D.; Yang, J.; Luo, D.; Xu, Z.; Wei, J.; Wang, J.-Q.; Xu, Z.; Peng, F.; et al. Chirality-specific growth of single-walled carbon nanotubes on solid alloy catalysts. *Nature* **2014**, *510*, 522–524, https://doi.org/10.1038/nature13434.
[35] Zhang, S.; Kang, L.; Wang, X.; Tong, L.; Yang, L.; Wang, Z.; Qi, K.; Deng, S.; Li, Q.; Bai, X.; et al. Arrays of horizontal carbon nanotubes of controlled chirality grown using designed catalysts. *Nature* **2017**, *543*, 234–238, https://doi.org/10.1038/nature21051.
[36] S.M. Bachilo, L. Balzano, J.E. Herrera, F. Pompeo, D.E. Resasco, R.B. Weisman, Narrow (n, m)-distribution of single-walled carbon nanotubes grown using a solid supported catalyst, J. Am. Chem. Soc. 125(37) (2003) 11186-11187.
[37] He, M.; Chernov, A.I.; Fedotov, P.V.; Obraztsova, E.D.; Sainio, J.; Rikkinen, E.; Jiang, H.; Zhu, Z.; Tian, Y.; Kauppinen, E.I.; et al. Predominant (6,5) Single-Walled Carbon Nanotube Growth on a Copper-Promoted Iron Catalyst. *J. Am. Chem. Soc.* **2010**, *132*, 13994–13996, https://doi.org/10.1021/ja106609y.
[38] Artyukhov, V.I.; Penev, E.S.; Yakobson, B.I. Why nanotubes grow chiral. *Nat. Commun.* **2014**, *5*, 4892, https://doi.org/10.1038/ncomms5892.
[39] Bati, A.S.R.; Yu, L.; Batmunkh, M.; Shapter, J.G. Synthesis, purification, properties and characterization of sorted single-walled carbon nanotubes. *Nanoscale* **2018**, *10*, 22087–22139, https://doi.org/10.1039/c8nr07379a.
[40] Yang, F.; Wang, M.; Zhang, D.; Yang, J.; Zheng, M.; Li, Y. Chirality Pure Carbon Nanotubes: Growth, Sorting, and Characterization. *Chem. Rev.* **2020**, *120*, 2693–2758, https://doi.org/10.1021/acs.chemrev.9b00835.
[41] Kharlamova, M.V.; Burdanova, M.G.; Paukov, M.I.; Kramberger, C. Synthesis, Sorting, and Applications of Single-Chirality Single-Walled Carbon Nanotubes. *Materials* **2022**, *15*, 5898, https://doi.org/10.3390/ma15175898.
[42] Iijima, S. Helical microtubules of graphitic carbon. *Nature* **1991**, *354*, 56–58, doi:10.1038/354056a0.
[43] Monthioux, M.; Kuznetsov, V.L. Who should be given the credit for the discovery of carbon nanotubes? *Carbon* **2006**, *44*, 1621–1623, https://doi.org/10.1016/j.carbon.2006.03.019.

[44] L. Radushkevich, V.O. Lukyanovich, strukture ugleroda, obrazujucegosja pri termiceskom razlozenii okisi ugleroda na zeleznom kontakte, Zurn. Fisic. Chim. 26 (1952) 88-95.
[45] Dai, H.; Rinzler, A.G.; Nikolaev, P.; Thess, A.; Colbert, D.T.; Smalley, R.E. Single-wall nanotubes produced by metal-catalyzed disproportionation of carbon monoxide. *Chem. Phys. Lett.* **1996**, *260*, 471–475, https://doi.org/10.1016/0009-2614(96)00862-7.
[46] Kong, J.; Cassell, A.M.; Dai, H. Chemical vapor deposition of methane for single-walled carbon nanotubes. *Chem. Phys. Lett.* **1998**, *292*, 567–574, https://doi.org/10.1016/s0009-2614(98)00745-3.
[47] E. Flahaut, A. Peigney, C. Laurent, A. Rousset, Synthesis of single-walled carbon nanotube-Co-MgO composite powders and extraction of the nanotubes, J. Mater. Chem. 10(2) (2000) 249-252.
[48] Qingwen, L.; Hao, Y.; Yan, C.; Jin, Z.; Zhongfan, L. A scalable CVD synthesis of high-purity single-walled carbon nanotubes with porous MgO as support material. *J. Mater. Chem.* **2002**, *12*, 1179–1183, https://doi.org/10.1039/b109763f.
[49] Li, Q.; Yan, H.; Zhang, J.; Liu, Z. Effect of hydrocarbons precursors on the formation of carbon nanotubes in chemical vapor deposition. *Carbon* **2004**, *42*, 829–835, https://doi.org/10.1016/j.carbon.2004.01.070.
[50] Bachilo, S.; Strano, M.; Kittrell, C.; Hauge, R.; Smalley, R.; Weisman, R. Structure-Assigned Optical Spectra of Single-Walled Carbon Nanotubes. *Science* **2002**, *298*, 2361–2366, https://doi.org/10.1126/science.1078727.
[51] O'Connell, M.J.; Bachilo, S.M.; Huffman, C.B.; Moore, V.C.; Strano, M.S.; Haroz, E.H.; Rialon, K.L.; Boul, P.J.; Noon, W.H.; Kittrell, C.; et al. Band Gap Fluorescence from Individual Single-Walled Carbon Nanotubes. *Science* **2002**, *297*, 593–596, https://doi.org/10.1126/science.1072631.
[52] Maruyama, S.; Miyauchi, Y.; Murakami, Y.; Chiashi, S. Optical characterization of single-walled carbon nanotubes synthesized by catalytic decomposition of alcohol. *New J. Phys.* **2003**, *5*, 149–149, https://doi.org/10.1088/1367-2630/5/1/149.
[53] He, M.; Li, D.; Yang, T.; Shang, D.; Chernov, A.I.; Fedotov, P.V.; Obraztsova, E.D.; Liu, Q.; Jiang, H.; Kauppinen, E. A robust CoxMg1-xO catalyst for predominantly growing (6, 5) single-walled carbon nanotubes. *Carbon* **2019**, *153*, 389–395, https://doi.org/10.1016/j.carbon.2019.07.050.
[54] Magnin, Y.; Amara, H.; Ducastelle, F.; Loiseau, A.; Bichara, C. Entropy-driven stability of chiral single-walled carbon nanotubes. *Science* **2018**, *362*, 212–215, https://doi.org/10.1126/science.aat6228.
[55] Lolli, G.; Zhang, L.; Balzano, L.; Sakulchaicharoen, N.; Tan, Y.; Resasco, D.E. Tailoring (*n*,*m*) Structure of Single-Walled Carbon Nanotubes by Modifying Reaction Conditions and the Nature of the Support of CoMo Catalysts. *J. Phys. Chem. B* **2006**, *110*, 2108–2115, https://doi.org/10.1021/jp056095e.
[56] Loebick, C.Z.; Podila, R.; Reppert, J.; Chudow, J.; Ren, F.; Haller, G.L.; Rao, A.M.; Pfefferle, L.D. Selective Synthesis of Subnanometer Diameter Semiconducting Single-Walled Carbon Nanotubes. *J. Am. Chem. Soc.* **2010**, *132*, 11125–11131, https://doi.org/10.1021/ja102011h.
[57] Li, X.; Tu, X.; Zaric, S.; Welsher, K.; Seo, W.S.; Zhao, W.; Dai, H. Selective Synthesis Combined with Chemical Separation of Single-Walled Carbon Nanotubes for Chirality Selection. *J. Am. Chem. Soc.* **2007**, *129*, 15770–15771, https://doi.org/10.1021/ja077886s.
[58] He, M.; Liu, B.; Chernov, A.I.; Obraztsova, E.D.; Kauppi, I.; Jiang, H.; Anoshkin, I.; Cavalca, F.; Hansen, T.W.; Wagner, J.B.; et al. Growth Mechanism of Single-Walled Carbon Nanotubes on Iron–Copper Catalyst and Chirality Studies by Electron Diffraction. *Chem. Mater.* **2012**, *24*, 1796–1801, https://doi.org/10.1021/cm300308k.
[59] Cantoro, M.; Hofmann, S.; Pisana, S.; Scardaci, V.; Parvez, A.; Ducati, C.; Ferrari, A.C.; Blackburn, A.M.; Wang, K.-Y.; Robertson, J. Catalytic Chemical Vapor Deposition of Single-Wall Carbon Nanotubes at Low Temperatures. *Nano Lett.* **2006**, *6*, 1107–1112, https://doi.org/10.1021/nl060068y.
[60] He, M.; Chernov, A.I.; Obraztsova, E.D.; Sainio, J.; Rikkinen, E.; Jiang, H.; Zhu, Z.; Kaskela, A.; Nasibulin, A.G.; Kauppinen, E.I.; et al. Low temperature growth of SWNTs on a nickel catalyst by thermal chemical vapor deposition. *Nano Res.* **2010**, *4*, 334–342, https://doi.org/10.1007/s12274-010-0088-3.
[61] Wu, Q.; Qiu, L.; Zhang, L.; Liu, H.; Ma, R.; Xie, P.; Liu, R.; Hou, P.; Ding, F.; Liu, C.; et al. Temperature-dependent selective nucleation of single-walled carbon nanotubes from stabilized catalyst nanoparticles. *Chem. Eng. J.* **2021**, *431*, 133487, https://doi.org/10.1016/j.cej.2021.133487.
[62] He, M.; Fedotov, P.V.; Chernov, A.; Obraztsova, E.D.; Jiang, H.; Wei, N.; Cui, H.; Sainio, J.; Zhang, W.; Jin, H.; et al. Chiral-selective growth of single-walled carbon nanotubes on Fe-based catalysts using CO as carbon source. *Carbon* **2016**, *108*, 521–528, https://doi.org/10.1016/j.carbon.2016.07.048.
[63] Miyauchi, Y.; Chiashi, S.; Murakami, Y.; Hayashida, Y.; Maruyama, S. Fluorescence spectroscopy of single-walled carbon nanotubes synthesized from alcohol. *Chem. Phys. Lett.* **2004**, *387*, 198–203, https://doi.org/10.1016/j.cplett.2004.01.116.
[64] Hou, B.; Wu, C.; Inoue, T.; Chiashi, S.; Xiang, R.; Maruyama, S. Extended alcohol catalytic chemical vapor deposition for efficient growth of single-walled carbon nanotubes thinner than (6,5). *Carbon* **2017**, *119*, 502–510, https://doi.org/10.1016/j.carbon.2017.04.045.

[65] Xiang, R.; Hou, B.; Einarsson, E.; Zhao, P.; Harish, S.; Morimoto, K.; Miyauchi, Y.; Chiashi, S.; Tang, Z.; Maruyama, S. Carbon Atoms in Ethanol Do Not Contribute Equally to Formation of Single-Walled Carbon Nanotubes. *ACS Nano* **2013**, *7*, 3095–3103, https://doi.org/10.1021/nn305180g.
[66] Xu, B.; Kaneko, T.; Shibuta, Y.; Kato, T. Preferential synthesis of (6,4) single-walled carbon nanotubes by controlling oxidation degree of Co catalyst. *Sci. Rep.* **2017**, *7*, 1–9, https://doi.org/10.1038/s41598-017-11712-0.
[67] Wang, B.; Poa, C.H.P.; Wei, L.; Li, L.-J.; Yang, Y.; Chen, Y. (*n*,*m*) Selectivity of Single-Walled Carbon Nanotubes by Different Carbon Precursors on Co−Mo Catalysts. *J. Am. Chem. Soc.* **2007**, *129*, 9014–9019, https://doi.org/10.1021/ja070808k.
[68] Moisala, A.; Nasibulin, A.G.; I Kauppinen, E. The role of metal nanoparticles in the catalytic production of single-walled carbon nanotubes—a review. *J. Physics: Condens. Matter* **2003**, *15*, S3011–S3035, https://doi.org/10.1088/0953-8984/15/42/003.
[69] Nasibulin, A.G.; Brown, D.P.; Queipo, P.; Gonzalez, D.; Jiang, H.; Kauppinen, E.I. An essential role of CO2 and H2O during single-walled CNT synthesis from carbon monoxide. *Chem. Phys. Lett.* **2006**, *417*, 179–184, https://doi.org/10.1016/j.cplett.2005.10.022.
[70] Gangoli, V.S.; Godwin, M.A.; Reddy, G.; Bradley, R.K.; Barron, A.R. The State of HiPco Single-Walled Carbon Nanotubes in 2019. *C* **2019**, *5*, 65, https://doi.org/10.3390/c5040065.
[71] A.G. Nasibulin, P.V. Pikhitsa, H. Jiang, D.P. Brown, A.V. Krasheninnikov, A. S. Anisimov, P. Queipo, A. Moisala. A novel hybrid carbon material. Nat. Nanotechnol 2(3) (2007) 156-161.
[72] He, M.; Jiang, H.; Kauppinen, E.I.; Lehtonen, J. Diameter and chiral angle distribution dependencies on the carbon precursors in surface-grown single-walled carbon nanotubes. *Nanoscale* **2012**, *4*, 7394–7398, https://doi.org/10.1039/c2nr32276e.
[73] He, M.; Magnin, Y.; Amara, H.; Jiang, H.; Cui, H.; Fossard, F.; Castan, A.; Kauppinen, E.; Loiseau, A.; Bichara, C. Linking growth mode to lengths of single-walled carbon nanotubes. *Carbon* **2017**, *113*, 231–236, https://doi.org/10.1016/j.carbon.2016.11.057.
[74] He, M.; Magnin, Y.; Jiang, H.; Amara, H.; Kauppinen, E.I.; Loiseau, A.; Bichara, C. Growth modes and chiral selectivity of single-walled carbon nanotubes. *Nanoscale* **2018**, *10*, 6744–6750, https://doi.org/10.1039/c7nr09539b.
[75] H.J. Grabke, Kinetics and mechanisms of surface-reactions occuring during carburization and decarburization and also nitrogenation and denitrogenation of iron in gases, Archiv. Eisenhuttenwes. 46 (1975) 75-81.
[76] M. He, X. Wang, S. Zhang, H. Jiang, F. Cavalca, H. Cui, J.B. Wagner, T.W. Hansen, E. Kauppinen, J. Zhang, Growth kinetics of single-walled carbon nanotubes with a (2n, n) chirality selection, Sci. Adv. 5(12) (2019) eaav9668.
[77] Chen, Y.; Ciuparu, D.; Lim, S.; Yang, Y.; Haller, G.L.; Pfefferle, L. Synthesis of uniform diameter single wall carbon nanotubes inBCo-MCM-41: effects of CO pressure and reaction time. *J. Catal.* **2004**, *226*, 351–362, https://doi.org/10.1016/j.jcat.2004.06.006.
[78] B. Wang, L. Wei, L. Yao, L.-J. Li, Y. Yang, Y. Chen, Pressure-induced single-walled carbon nanotube (n, m) selectivity on Co-Mo catalysts, J. Phys. Chem. C 111(40) (2007) 14612-14616.
[79] Li, Y.; Kim, W.; Zhang, Y.; Rolandi, M.; Wang, D.; Dai, H. Growth of Single-Walled Carbon Nanotubes from Discrete Catalytic Nanoparticles of Various Sizes. *J. Phys. Chem. B* **2001**, *105*, 11424–11431, https://doi.org/10.1021/jp012085b.
[80] Cheung, C.L.; Kurtz, A.; Park, H.; Lieber, C.M. Diameter-Controlled Synthesis of Carbon Nanotubes. *J. Phys. Chem. B* **2002**, *106*, 2429–2433, https://doi.org/10.1021/jp0142278.
[81] An, L.; Owens, J.M.; McNeil, L.E.; Liu, J. Synthesis of Nearly Uniform Single-Walled Carbon Nanotubes Using Identical Metal-Containing Molecular Nanoclusters as Catalysts. *J. Am. Chem. Soc.* **2002**, *124*, 13688–13689, https://doi.org/10.1021/ja0274958.
[82] Lv, S.; Wu, Q.; Xu, Z.; Yang, T.; Jiang, K.; He, M. Chirality distribution of single-walled carbon nanotubes grown from gold nanoparticles. *Carbon* **2022**, *192*, 259–264, https://doi.org/10.1016/j.carbon.2022.02.051.
[83] R.E. Smalley, Y. Li, V.C. Moore, B. K. Price, R. Colorado, H.K. Schmidt, R.H. Hauge, A. R. Barron, J. M. Tour. Single wall carbon nanotube amplification: En route to a type-specific growth mechanism[J]. J. Am. Chem. Soc. 128(49) (2006) 15824-15829.
[84] Y. Yao, C. Feng, J. Zhang, Z. Liu. "Cloning" of single-walled carbon nanotubes via open-end growth mechanism. Nano Lett. 9(4) (2009) 1673-1677.
[85] Yu, X.; Zhang, J.; Choi, W.; Choi, J.-Y.; Kim, J.M.; Gan, L.; Liu, Z. Cap Formation Engineering: From Opened C_{60} to Single-Walled Carbon Nanotubes. *Nano Lett.* **2010**, *10*, 3343–3349, https://doi.org/10.1021/nl1010178.
[86] Liu, J.; Wang, C.; Tu, X.; Liu, B.; Chen, L.; Zheng, M.; Zhou, C. Chirality-controlled synthesis of single-wall carbon nanotubes using vapour-phase epitaxy. *Nat. Commun.* **2012**, *3*, 1199, https://doi.org/10.1038/ncomms2205.

[87] Omachi, H.; Nakayama, T.; Takahashi, E.; Segawa, Y.; Itami, K. Initiation of carbon nanotube growth by well-defined carbon nanorings. *Nat. Chem.* **2013**, *5*, 572–576, https://doi.org/10.1038/nchem.1655.
[88] J.R. Sanchez-Valencia, T. Dienel, O. Gröning, I. Shorubalko, A. Mueller, M. Jansen, K. Amsharov, P. Ruffieux, R. Fasel. Contorlled synthesis of single-chirality carbon nanotubes. Nature 512(7512) (2014) 61-64.
[89] He, M.; Jin, H.; Zhang, L.; Jiang, H.; Yang, T.; Cui, H.; Fossard, F.; Wagner, J.B.; Karppinen, M.; Kauppinen, E.I.; et al. Environmental transmission electron microscopy investigations of Pt-Fe2O3 nanoparticles for nucleating carbon nanotubes. *Carbon* **2016**, *110*, 243–248, https://doi.org/10.1016/j.carbon.2016.09.026.
[90] M. He, X. Wang, S. Zhang, H. Jiang, F. Cavalca, H. Cui, J.B. Wagner, T.W. Hansen, E. Kauppinen, J. Zhang, F. Ding. Growth kinetics of single-walled carbon nanotubes with a (2 n, n) chirality selection[J]. Sci. Adv. 5(12) (2019) eaav9668.
[91] Ding, F.; Larsson, P.; Larsson, J.A.; Ahuja, R.; Duan, H.; Rosén, A.; Bolton, K. The Importance of Strong Carbon−Metal Adhesion for Catalytic Nucleation of Single-Walled Carbon Nanotubes. *Nano Lett.* **2007**, *8*, 463–468, https://doi.org/10.1021/nl072431m.
[92] Yazyev, O.V.; Pasquarello, A. Effect of Metal Elements in Catalytic Growth of Carbon Nanotubes. *Phys. Rev. Lett.* **2008**, *100*, 156102, https://doi.org/10.1103/physrevlett.100.156102.
[93] Takagi, D.; Homma, Y.; Hibino, H.; Suzuki, S.; Kobayashi, Y. Single-Walled Carbon Nanotube Growth from Highly Activated Metal Nanoparticles. *Nano Lett.* **2006**, *6*, 2642–2645, https://doi.org/10.1021/nl061797g.
[94] Yuan, D.; Ding, L.; Chu, H.; Feng, Y.; McNicholas, T.P.; Liu, J. Horizontally Aligned Single-Walled Carbon Nanotube on Quartz from a Large Variety of Metal Catalysts. *Nano Lett.* **2008**, *8*, 2576–2579, https://doi.org/10.1021/nl801007r.
[95] Resasco, D.; Alvarez, W.; Pompeo, F.; Balzano, L.; Herrera, J.; Kitiyanan, B.; Borgna, A. A Scalable Process for Production of Single-walled Carbon Nanotubes (SWNTs) by Catalytic Disproportionation of CO on a Solid Catalyst. *J. Nanoparticle Res.* **2002**, *4*, 131–136, https://doi.org/10.1023/a:1020174126542.
[96] Alvarez, W.; Kitiyanan, B.; Borgna, A.; Resasco, D. Synergism of Co and Mo in the catalytic production of single-wall carbon nanotubes by decomposition of CO. *Carbon* **2001**, *39*, 547–558, https://doi.org/10.1016/s0008-6223(00)00173-1.
[97] Lim, S.; Ciuparu, D.; Pak, C.; Dobek, F.; Chen, Y.; Harding, D.; Pfefferle, L.; Haller, G. Synthesis and Characterization of Highly Ordered Co−MCM-41 for Production of Aligned Single Walled Carbon Nanotubes (SWNT). *J. Phys. Chem. B* **2003**, *107*, 11048–11056, https://doi.org/10.1021/jp0304778.
[98] Ciuparu, D.; Chen, Y.; Lim, S.; Haller, G.L.; Pfefferle, L. Uniform-Diameter Single-Walled Carbon Nanotubes Catalytically Grown in Cobalt-Incorporated MCM-41. *J. Phys. Chem. B* **2003**, *108*, 503–507, https://doi.org/10.1021/jp036453i.
[99] He, M.; Chernov, A.I.; Fedotov, P.V.; Obraztsova, E.D.; Rikkinen, E.; Zhu, Z.; Sainio, J.; Jiang, H.; Nasibulin, A.G.; Kauppinen, E.I.; et al. Selective growth of SWNTs on partially reduced monometallic cobalt catalyst. *Chem. Commun.* **2010**, *47*, 1219–1221, https://doi.org/10.1039/c0cc02751k.
[100] Li, N.; Wang, X.; Derrouiche, S.; Haller, G.L.; Pfefferle, L.D. Role of Surface Cobalt Silicate in Single-Walled Carbon Nanotube Synthesis from Silica-Supported Cobalt Catalysts. *ACS Nano* **2010**, *4*, 1759–1767, https://doi.org/10.1021/nn901812t.
[101] Lim, S.; Wang, C.; Yang, Y.; Ciuparu, D.; Pfefferle, L.; Haller, G.L. Evidence for anchoring and partial occlusion of metallic clusters on the pore walls of MCM-41 and effect on the stability of the metallic clusters. *Catal. Today* **2007**, *123*, 122–132, https://doi.org/10.1016/j.cattod.2007.03.005.
[102] Li, N.; Wang, X.; Ren, F.; Haller, G.L.; Pfefferle, L.D. Diameter Tuning of Single-Walled Carbon Nanotubes with Reaction Temperature Using a Co Monometallic Catalyst. *J. Phys. Chem. C* **2009**, *113*, 10070–10078, https://doi.org/10.1021/jp903129h.
[103] He, M.; Jiang, H.; Liu, B.; Fedotov, P.V.; Chernov, A.I.; Obraztsova, E.D.; Cavalca, F.; Wagner, J.B.; Hansen, T.W.; Anoshkin, I.V.; et al. Chiral-Selective Growth of Single-Walled Carbon Nanotubes on Lattice-Mismatched Epitaxial Cobalt Nanoparticles. *Sci. Rep.* **2013**, *3*, srep01460, https://doi.org/10.1038/srep01460.
[104] He, M.; Jiang, H.; Kauppi, I.; Fedotov, P.V.; Chernov, A.I.; Obraztsova, E.D.; Cavalca, F.; Wagner, J.B.; Hansen, T.W.; Sainio, J.; et al. Insights into chirality distributions of single-walled carbon nanotubes grown on different $Co_xMg_{1-x}O$ solid solutions. *J. Mater. Chem. A* **2014**, *2*, 5883–5889, https://doi.org/10.1039/c3ta15325h.
[105] Wang, H.; Wang, B.; Quek, X.-Y.; Wei, L.; Zhao, J.; Li, L.-J.; Chan-Park, M.B.; Yang, Y.; Chen, Y. Selective Synthesis of (9,8) Single Walled Carbon Nanotubes on Cobalt Incorporated TUD-1 Catalysts. *J. Am. Chem. Soc.* **2010**, *132*, 16747–16749, https://doi.org/10.1021/ja106937y.
[106] H. Wang, L. Wei, F. Ren, Q. Wang, L.D. Pfefferle, G.L. Haller, Y. Chen, Chiral-selective CoSO4/SiO2 catalyst for (9, 8) single-walled carbon nanotube growth, ACS Nano 7(1) (2012) 614-626.

[107] Y. Yuan, H.E. Karahan, C. Yıldırım, L. Wei, Ö. Birer, S. Zhai, R. Lau, Y. Chen, "Smart poisoning" of Co/SiO2 catalysts by sulfidation for chirality-selective synthesis of (9, 8) single-walled carbon nanotubes, Nanoscale 8(40) (2016) 17705-17713.
[108] Loebick, C.Z.; Derrouiche, S.; Marinkovic, N.; Wang, C.; Hennrich, F.; Kappes, M.M.; Haller, G.L.; Pfefferle, L.D. Effect of Manganese Addition to the Co-MCM-41 Catalyst in the Selective Synthesis of Single Wall Carbon Nanotubes. *J. Phys. Chem. C* **2009**, *113*, 21611–21620, https://doi.org/10.1021/jp908262u.
[109] Loebick, C.Z.; Derrouiche, S.; Fang, F.; Li, N.; Haller, G.L.; Pfefferle, L.D. Effect of chromium addition to the Co-MCM-41 catalyst in the synthesis of single wall carbon nanotubes. *Appl. Catal. A: Gen.* **2009**, *368*, 40–49, https://doi.org/10.1016/j.apcata.2009.08.004.
[110] Ago, H.; Imamura, S.; Okazaki, T.; Saito, T.; Yumura, M.; Tsuji, M. CVD Growth of Single-Walled Carbon Nanotubes with Narrow Diameter Distribution over Fe/MgO Catalyst and Their Fluorescence Spectroscopy. *J. Phys. Chem. B* **2005**, *109*, 10035–10041, https://doi.org/10.1021/jp050307q.
[111] He, M.; Wang, Y.; Zhang, X.; Zhang, H.; Meng, Y.; Shang, D.; Xue, H.; Li, D.; Wu, Z. Stability of iron-containing nanoparticles for selectively growing single-walled carbon nanotubes. *Carbon* **2019**, *158*, 795–801, https://doi.org/10.1016/j.carbon.2019.11.056.
[112] F. Han, L. Qian, Q. Wu, D. Li, S. Hao, L. Feng, L. Xin, T. Yang, J. Zhang, M. He, Narrow-chirality distributed single-walled carbon nanotube synthesized from oxide promoted Fe-SiC catalyst, Carbon 191 (2022) 146-152.
[113] Wu, Q.; Zhang, H.; Ma, C.; Li, D.; Xin, L.; Zhang, X.; Zhao, N.; He, M. SiO2-promoted growth of single-walled carbon nanotubes on an alumina supported catalyst. *Carbon* **2021**, *176*, 367–373, https://doi.org/10.1016/j.carbon.2021.01.143.
[114] Yang, Y.; Lim, S.; Du, G.; Chen, Y.; Ciuparu, D.; Haller, G.L. Synthesis and Characterization of Highly Ordered Ni-MCM-41 Mesoporous Molecular Sieves. *J. Phys. Chem. B* **2005**, *109*, 13237–13246, https://doi.org/10.1021/jp044227i.
[115] Chiang, W.-H.; Sankaran, R.M. Linking catalyst composition to chirality distributions of as-grown single-walled carbon nanotubes by tuning NixFe1−x nanoparticles. *Nat. Mater.* **2009**, *8*, 882–886, https://doi.org/10.1038/nmat2531.
[116] He, M.; Wang, X.; Zhang, L.; Wu, Q.; Song, X.; Chernov, A.I.; Fedotov, P.V.; Obraztsova, E.D.; Sainio, J.; Jiang, H.; et al. Anchoring effect of Ni2+ in stabilizing reduced metallic particles for growing single-walled carbon nanotubes. *Carbon* **2018**, *128*, 249–256, https://doi.org/10.1016/j.carbon.2017.11.093.
[117] Murakami, Y.; Miyauchi, Y.; Chiashi, S.; Maruyama, S. Characterization of single-walled carbon nanotubes catalytically synthesized from alcohol. *Chem. Phys. Lett.* **2003**, *374*, 53–58, https://doi.org/10.1016/s0009-2614(03)00687-0.
[118] Hao, S.; Qian, L.; Wu, Q.; Li, D.; Han, F.; Feng, L.; Xin, L.; Yang, T.; Wang, S.; Zhang, J.; et al. Subnanometer Single-Walled carbon nanotube growth from Fe-Containing Layered double hydroxides. *Chem. Eng. J.* **2022**, *446*, https://doi.org/10.1016/j.cej.2022.137087.
[119] Robertson, J. Heterogeneous catalysis model of growth mechanisms of carbon nanotubes, graphene and silicon nanowires. *J. Mater. Chem.* **2012**, *22*, 19858–19862, https://doi.org/10.1039/c2jm33732k.
[120] Silvearv, F.; Larsson, P.; Jones, S.L.T.; Ahuja, R.; Larsson, J.A. Establishing the most favorable metal–carbon bond strength for carbon nanotube catalysts. *J. Mater. Chem. C* **2015**, *3*, 3422–3427, https://doi.org/10.1039/c5tc00143a.
[121] Maruyama, T. Current status of single-walled carbon nanotube synthesis from metal catalysts by chemical vapor deposition. *Mater. Express* **2018**, *8*, 1–20, https://doi.org/10.1166/mex.2018.1407.
[122] Takagi, D.; Homma, Y.; Hibino, H.; Suzuki, S.; Kobayashi, Y. Single-Walled Carbon Nanotube Growth from Highly Activated Metal Nanoparticles. *Nano Lett.* **2006**, *6*, 2642–2645, https://doi.org/10.1021/nl061797g.
[123] Zhang, X.; Qian, L.; Yao, X.; Zhang, L.; Wu, Q.; Li, D.; Ma, C.; Zhao, N.; Xin, L.; Liu, C.; et al. Solid supported ruthenium catalyst for growing single-walled carbon nanotubes with narrow chirality distribution. *Carbon* **2022**, *193*, 35–41, https://doi.org/10.1016/j.carbon.2022.03.010.
[124] Ma, C.; Liu, Y.; Zhang, L.; Qian, L.; Zhao, Y.; Tian, Y.; Wu, Q.; Li, D.; Zhao, N.; Zhang, X.; et al. Bulk growth and separation of single-walled carbon nanotubes from rhenium catalyst. *Nano Res.* **2022**, *15*, 5775–5780, https://doi.org/10.1007/s12274-022-4248-z.
[125] Qin, X.; Li, D.; Feng, L.; Wang, Y.; Zhang, L.; Qian, L.; Zhao, W.; Xu, N.; Chi, X.; Wang, S.; et al. (n, m) Distribution of Single-Walled Carbon Nanotubes Grown from a Non-Magnetic Palladium Catalyst. *Molecules* **2023**, *28*, 2453, https://doi.org/10.3390/molecules28062453.
[126] Ding, F.; Harutyunyan, A.R.; Yakobson, B.I. Dislocation theory of chirality-controlled nanotube growth. *Proc. Natl. Acad. Sci.* **2009**, *106*, 2506–2509, https://doi.org/10.1073/pnas.0811946106.

[127] Wu, Q.; Ji, Z.; Xin, L.; Li, D.; Zhang, L.; Liu, C.; Yang, T.; Wen, Z.; Wang, H.; Xin, B.; et al. Iron silicide-catalyzed growth of single-walled carbon nanotubes with a narrow diameter distribution. *Carbon* **2019**, *149*, 139–143, https://doi.org/10.1016/j.carbon.2019.04.059.
[128] Yang, F.; Wang, X.; Zhang, D.; Qi, K.; Yang, J.; Xu, Z.; Li, M.; Zhao, X.; Bai, X.; Li, Y. Growing Zigzag (16,0) Carbon Nanotubes with Structure-Defined Catalysts. *J. Am. Chem. Soc.* **2015**, *137*, 8688–8691, https://doi.org/10.1021/jacs.5b04403.
[129] Zhao, Q.; Xu, Z.; Hu, Y.; Ding, F.; Zhang, J. Chemical vapor deposition synthesis of near-zigzag single-walled carbon nanotubes with stable tube-catalyst interface. *Sci. Adv.* **2016**, *2*, e1501729–1501729, https://doi.org/10.1126/sciadv.1501729.
[130] X. Wei, S. Li, W. Wang, X. Zhang, W. Zhou, S. Xie, H. Liu. Recent Advances in Structure Separation of Single-Wall Carbon Nanotubes and Their Application in Optics, Electronics, and Optoelectronics. Adv. Sci. 9(14) (2022) 2200054.
[131] Y. Li, M. Zheng, J. Yao, W. Gong, Y. Li, J. Tang, S. Feng, R. Han, Q. Sui, S. Qiu, L. Kang, H. Jin, D. Sun, Q. Li. High-purity monochiral carbon nanotubes with a 1.2 nm diameter for high-performance field-effect transistors. Adv. Funct. Mater. 32(1) (2022) 2107119.
[132] H. Maune, S. Han. DNA-directed self-assembly of highly ordered and dense single-walled carbon nanotube arrays. Methods Mol. Biol (2017) 245-256.
[133] Chen, Z.; Appenzeller, J.; Knoch, J.; Lin, Y.-M.; Avouris, P. The Role of Metal−Nanotube Contact in the Performance of Carbon Nanotube Field-Effect Transistors. *Nano Lett.* **2005**, *5*, 1497–1502, https://doi.org/10.1021/nl0508624.
[134] Wang, Y.; Liu, D.; Zhang, H.; Wang, J.; Du, R.; Li, T.-T.; Qian, J.; Hu, Y.; Huang, S. Methylation-Induced Reversible Metallic-Semiconducting Transition of Single-Walled Carbon Nanotube Arrays for High-Performance Field-Effect Transistors. *Nano Lett.* **2019**, *20*, 496–501, https://doi.org/10.1021/acs.nanolett.9b04219.